Wind speed reductions by large-scale wind turbine deployments lower turbine efficiencies and set low generation limits

Lee M. Miller[a,1,2] and Axel Kleidon[a]

[a]Biospheric Theory and Modelling, Max Planck Institute for Biogeochemistry, D-07701 Jena, Germany

Edited by Kerry A. Emanuel, Massachusetts Institute of Technology, Cambridge, MA, and approved September 23, 2016 (received for review February 9, 2016)

Wind turbines generate electricity by removing kinetic energy from the atmosphere. Large numbers of wind turbines are likely to reduce wind speeds, which lowers estimates of electricity generation from what would be presumed from unaffected conditions. Here, we test how well wind power limits that account for this effect can be estimated without explicitly simulating atmospheric dynamics. We first use simulations with an atmospheric general circulation model (GCM) that explicitly simulates the effects of wind turbines to derive wind power limits (GCM estimate), and compare them to a simple approach derived from the climatological conditions without turbines [vertical kinetic energy (VKE) estimate]. On land, we find strong agreement between the VKE and GCM estimates with respect to electricity generation rates (0.32 and 0.37 W_e m^{-2}) and wind speed reductions by 42 and 44%. Over ocean, the GCM estimate is about twice the VKE estimate (0.59 and 0.29 W_e m^{-2}) and yet with comparable wind speed reductions (50 and 42%). We then show that this bias can be corrected by modifying the downward momentum flux to the surface. Thus, large-scale limits to wind power use can be derived from climatological conditions without explicitly simulating atmospheric dynamics. Consistent with the GCM simulations, the approach estimates that only comparatively few land areas are suitable to generate more than 1 W_e m^{-2} of electricity and that larger deployment scales are likely to reduce the expected electricity generation rate of each turbine. We conclude that these atmospheric effects are relevant for planning the future expansion of wind power.

momentum | natural limits | surface stress | wind energy | vertical transport

Wind power is a renewable energy source that could meet the primary human energy demand with extensive large-scale deployment. Over the last decade, wind power deployment has increased by 23% per year, contributing 2.2% of the global electricity demand in 2010 and 3.7% in 2014 (1). Many governments are pursuing ambitious plans to further increase the proportion of wind energy within their energy systems. By 2035, the International Energy Agency predicts that even with the projected increase in global electricity demand to 2.6–4.3 terawatts (TW_e = 10^{12} watts of electricity), wind power is projected to contribute 22–28% (0.95–1.2 TW_e) of this electricity demand (2).

Plans for future wind power deployment are commonly derived from observed wind speeds in combination with assumed turbine characteristics and spacing (e.g., refs. 3–5). However, this approach is only applicable for a few isolated wind turbines or when a row of wind turbines are aligned perpendicular to the wind direction (common offshore). Increasing wind turbine deployment uses an increasing share of the kinetic energy of the atmosphere, thus likely slowing down wind speeds. Climate models can explicitly simulate these effects (6–8) and yield a 10-fold reduction of the expected large-scale electricity generation rate from 3 to 5 W_e m^{-2} reported in studies using observed wind speeds (3–5, 9, 10) down to 0.3–0.5 W_e m^{-2} reported in climate model studies (6–8), with about 1.0 W_e m^{-2} possible in more windy regions like the US Midwest (6, 8, 11–13).

However, climate models are inherently complex and computationally intense and do not allow for the use of observed wind fields to derive limits for large-scale wind power use. Ideally, one would combine the effect of reduced wind speeds with the realism of observed wind fields and thereby obtain better estimates of wind power limits of different regions. Here, we present such an approach, test it against climate model simulations for different regions across land and ocean, and evaluate the implications of atmospheric effects on the electricity generation rate of individual wind turbines. Our approach uses the atmospheric momentum balance as the physical basis to predict how wind speeds decline in the presence of wind turbines. This approach therefore includes the effect that more wind turbines lower wind speeds, yielding the limit (or maximum rate) of kinetic energy that can theoretically be extracted from the atmosphere by the turbines. This approach [vertical kinetic energy (VKE) (6, 7, 13)] thus estimates the large-scale limit of wind power generation within a region.

The goal here is to evaluate the broader geographic applicability of the VKE approach over a range of climatic conditions by comparing VKE estimates to those simulated by a general circulation model (GCM) with various intensities of wind power deployment. We then modify VKE to improve the agreement with the GCM estimate, referring to it as the mVKE approach. Not only do the wind power limits predicted by mVKE and the GCM approach match within a factor of 2, but they also agree well with previously published estimates using other GCMs (6, 8, 11, 14). These mVKE estimates are substantially lower than estimates based only on observed wind speed and technical characteristics of

Significance

Understanding the limits of electricity generation from winds is a requirement for planning a renewable energy future. A difficulty in estimating such limits is that wind turbines remove kinetic energy from the atmosphere, so that many turbines should reduce wind speeds, ultimately setting a limit to how much kinetic energy can be taken out of the atmosphere. We show that this slowdown effect can be accounted for by detailed climate model simulations and a relatively simple method that does not directly simulate atmospheric dynamics. This slowdown effect is critical to consider, as it makes each turbine less productive and shows that few land areas can yield more than 1.0 W_e m^{-2} of electricity at large scales.

Author contributions: L.M.M. and A.K. designed research, performed research, analyzed data, and wrote the paper.

The authors declare no conflict of interest.

This article is a PNAS Direct Submission.

Freely available online through the PNAS open access option.

[1]Present address: Harvard John A. Paulson School of Engineering and Applied Sciences, Harvard University, Cambridge, MA 02138.

[2]To whom correspondence should be addressed. Email: lmiller@seas.harvard.edu.

This article contains supporting information online at www.pnas.org/lookup/suppl/doi:10.1073/pnas.1602253113/-/DCSupplemental.

the turbines (3–5, 15). The reduction in wind speeds plays a central role in shaping these lower estimates: it directly impacts the electricity generation rate of each turbine, regardless of its technical design. We then discuss that including these atmospheric effects is critical to planning for the expansion of large-scale wind power.

Methods

We evaluate wind power limits at large scales in the climatological mean using two approaches: the GCM and VKE approaches. In the GCM approach, the Planet Simulator GCM of the atmosphere (16, 17) is used for sensitivity simulations of a wide range of installed capacities (0.02–1360 $MW_i\ km^{-2}$) at the global scale, similar to previous studies (6–8, 11–14). The effect of wind turbines is described by an additional drag component in the surface momentum flux in the model. This added drag in combination with the simulated wind speeds is then used to estimate the rate of electricity generation by the wind turbines. From our simulated range of installed capacities, we then identify the maximum electric energy generation rate over land and ocean, and refer to it as the "GCM" estimate.

In the VKE approach, the wind speeds (v_0) and surface momentum fluxes (τ_0) from the control simulation of the GCM without turbines (indicated by the subscript 0) are used to estimate the large-scale wind power limit. The VKE estimate uses the maximum electricity generation rate at large-scale, described by $G_{e,VKE} = (4\sqrt{3})/27 \cdot \tau_0 \cdot v_0$. Note that this expression only uses the natural conditions of the control climate and no technical specifications. This limit is associated with a reduction in wind speeds by $1 - (\sqrt{3})/3 \cdot v_0 = 42\%$ or to $58\% \cdot v_0$, which is a direct consequence of the kinetic energy extraction by the wind turbines in combination with the momentum balance of the lower atmosphere. To improve the agreement with the GCM estimate, we then derive a correction $\tau_m = f(\tau_0)$, whereas the velocity reduction is given by the same expression as above. This correction yields a modified estimate of $G_{e,mVKE} = (4\sqrt{3})/27 \cdot \tau_m \cdot v_0$, where τ_m is the modified surface momentum flux. We refer to this modified estimate as the mVKE estimate. More details on the methodology are provided in *SI Appendix*.

Results and Discussion

We first identify the wind power limits within the GCM sensitivity simulations and the associated changes in wind speeds (Fig. 1). Fig. 1*A* shows the mean electricity generation rates simulated at progressively higher installed capacities. As would be expected, electricity generation first increases with greater installed capacity but then reaches a maximum rate of about 0.37 $W_e\ m^{-2}$ on land (0.59 $W_e\ m^{-2}$ over ocean) at an installed capacity of 24.3 $MW_i\ km^{-2}$ on land (9.1 $MW_i\ km^{-2}$ over ocean). Note that the generation rate does not "saturate," as suggested by ref. 8, but rather generation reaches a maximum limit, beyond which electricity generation is reduced due to the further slowdown in wind speeds (6, 7, 13).

This reduction in wind speeds with greater installed capacities is shown in Fig. 1*B*. Compared with the control climate without turbines, the wind speed is reduced from a mean of 4.6 m s^{-1} on land (7.8 m s^{-1} over ocean) to 2.6 m s^{-1} at the maximum (3.9 m s^{-1} over ocean), which represents a decrease by 44% (50%). Note that these generation rates and wind speed reductions show a large extent of spatial variation (Fig. 2 *C* and *D*) and temporal variation that is not discernible in the means shown in Fig. 1.

These estimates compare well to previous studies (Table 1). When averaged over the whole globe, our GCM simulations yield a mean maximum rate of 0.53 $W_e\ m^{-2}$ (270 TW_e), which is comparable to previous model-based estimates of 0.44–0.55 $W_e\ m^{-2}$ (224–282 TW_e; rows n and o in Table 1) (8, 14). Over land, our GCM estimate of 0.37 $W_e\ m^{-2}$ (49 TW_e) compares well to the range of 0.26–0.54 $W_e\ m^{-2}$ (34–71 TW_e; rows q–s in Table 1) (6, 8, 19). The GCM-based estimates reproduce the higher generation rates of the US Midwest and Western Europe at about 1 $W_e\ m^{-2}$ (Fig. 2*C*) (6–8, 11–13). The ocean estimates also agree broadly in magnitude [rows v and w in Table 1 (8), as well as being visually comparable to the simulations by ref. 14]. All of these generation rates are lower than large-scale estimates of 3–6 $W_e\ m^{-2}$ derived in studies that used observed wind speeds ("climatology-based estimates"; rows c, f, h, j, and k in Table 1). Note that these climatology-based estimates are about 10 times higher than GCM-based estimates and the mVKE estimate because previous climatology-based estimates neglected the slowdown effect.

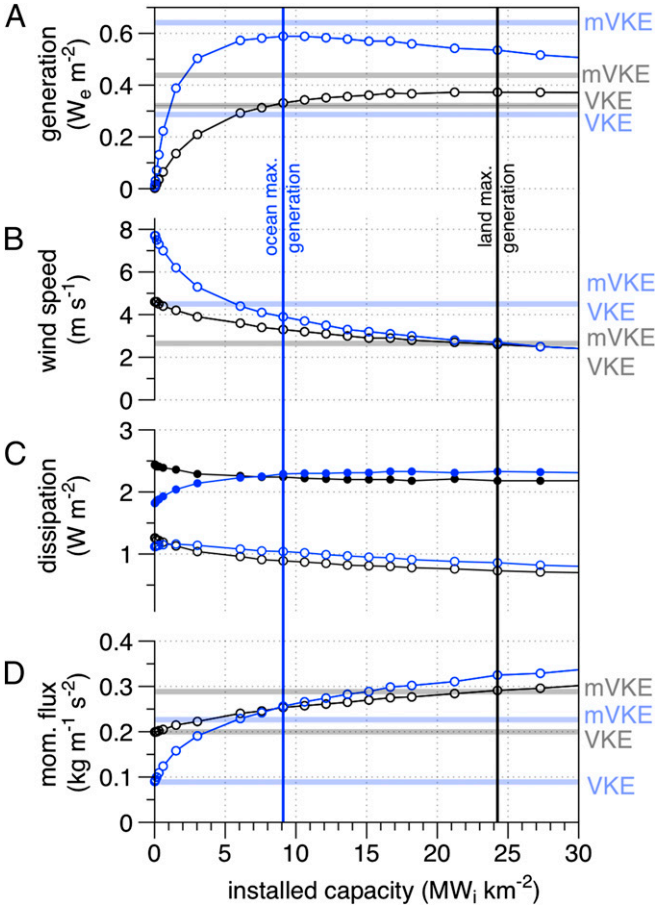

Fig. 1. Simulated global-scale sensitivity of annual means of the rate of electricity generation (*A*), wind speed (*B*), dissipation of the total atmosphere (solid points) and near the surface (open points) (*C*), and (*D*) downward flux of horizontal momentum to the installed capacity of wind turbines for ocean (blue) and land (black). The vertical lines mark the installed capacities that yield maximum generation rates over ocean (9 $MW_i\ km^{-2}$) or land (24 $MW_i\ km^{-2}$). The horizontal lines show the values estimated or used by the VKE and mVKE approaches (blue for ocean; black for land).

Also consistent with previous estimates is the total dissipation rate, shown in Fig. 1*C*. As dissipation balances the kinetic energy generation in the climatological mean, it provides an estimate of kinetic energy generation of about 2.5 W m^{-2}, which sustains atmospheric motion. This rate is consistent with long-standing estimates of 2–3 W m^{-2} derived from atmospheric energetics (22, 23). About half of the generated kinetic energy is dissipated near the surface, with a mean value of about 1.2 W m^{-2} (Fig. 1*C*, open circles). Dissipation near the surface decreases because wind speeds are reduced with greater installed capacity, but total atmospheric dissipation remains almost constant. This finding indicates that dissipation is being shifted aloft to higher altitudes in the lower atmosphere. The limit to wind power generation in our simulations is thus below the ~1.2 W m^{-2} dissipation rate of the lower atmosphere, consistent with what has been proposed previously (18).

We next evaluate how well these estimates are predicted from the climatic conditions of the control simulation by the VKE approach. The inputs of VKE are wind speed and surface momentum flux, and the resulting estimates are shown in Fig. 1 (also see rows a, e, i, and l in Table 1). The VKE estimates are within a factor of 2 of the GCM estimates over 87% of the land surface (*SI Appendix*, Fig. S3), with VKE yielding a mean of

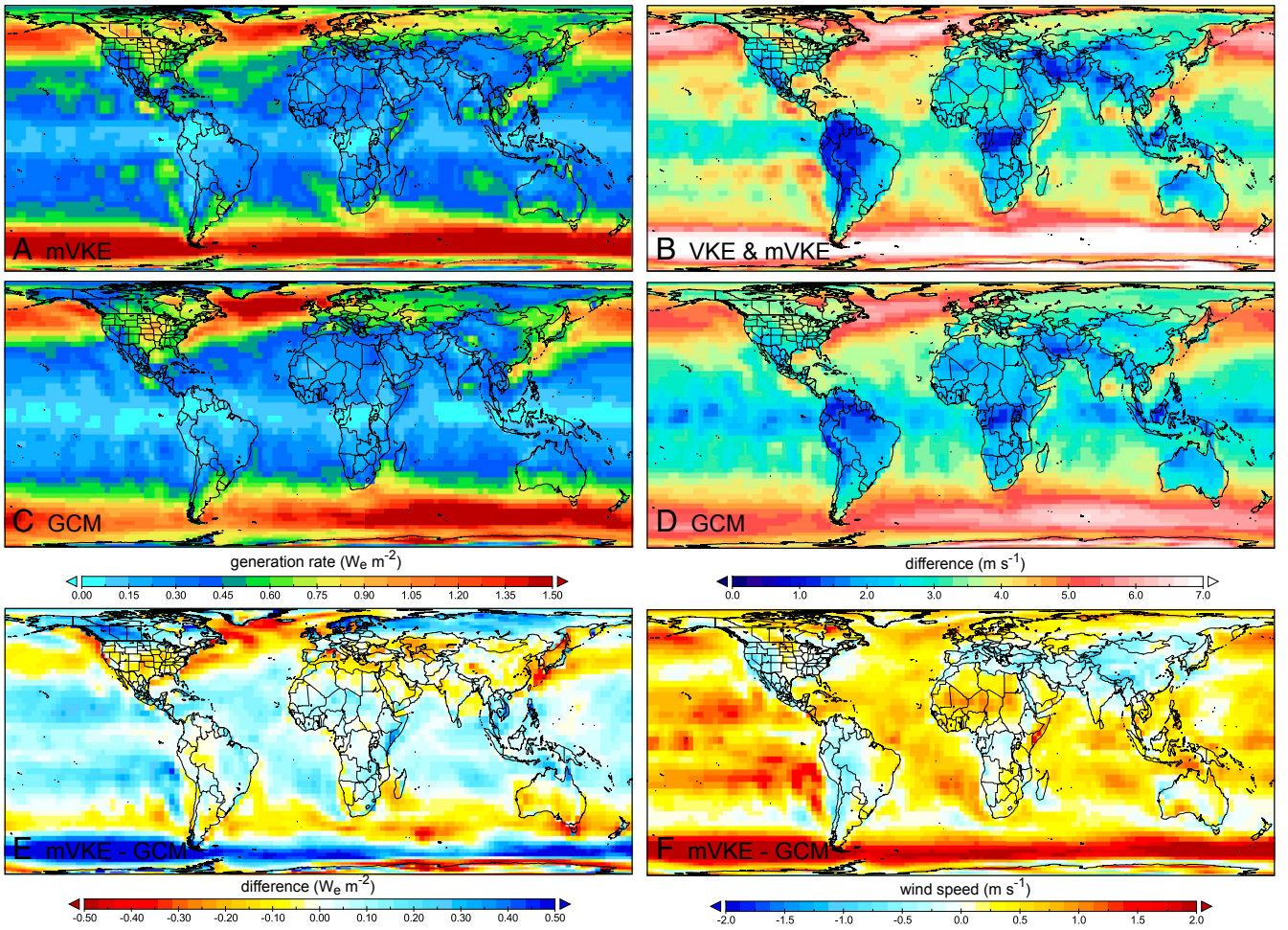

Fig. 2. Annual means of the maximum electricity generation rate estimated by the mVKE (*A*) and GCM (*C*) approaches, as well as the associated wind speeds from mVKE (*B*) and GCM (*D*). *E* and *F* show the differences between the mVKE and GCM approaches.

0.32 W_e m^{-2}, whereas the GCM yields 0.37 W_e m^{-2}. The agreement over the ocean is not as good (*SI Appendix*, Fig. S3), with 33% of the ocean estimates within a factor of 2 (*SI Appendix*, Fig. S3), and VKE underestimating the mean (0.29 W_e m^{-2}) in comparison with the GCM (0.59 W_e m^{-2}).

We next look at two factors that shape the VKE estimate to understand the reason for this bias: wind speed and downward flux of horizontal momentum to the surface. VKE adequately captures the decrease in wind speed by 42% over land and ocean, which compares well with the GCM-based estimate of 44 and 50%, respectively (Fig. 1*B*). The spatial distribution of the reduction in wind speeds by VKE and the GCM also agree reasonably well (Fig. 2*C*, Fig. 3*B*, and statistical relationships in *SI Appendix*, *Supplement C*). This agreement is found over both land and ocean, although the magnitude is somewhat better reproduced over land. The underestimation by VKE is therefore not due to a general bias in estimating the wind speed reduction. Therefore, we attribute this deviation to the wind turbines enhancing the downward momentum flux.

The underestimation of VKE over oceans results from a substantial increase in the downward momentum flux (Fig. 1*D*), whereas VKE assumes this flux to remain unaffected. Comparing the control climate to the simulation at maximum wind power, over land, the downward momentum flux increases by 45% (0.20 to 0.29 kg m^{-1} s^{-2}), but over ocean, the flux nearly triples (+188%, 0.09 to 0.26 kg m^{-1} s^{-2}; *SI Appendix*, Fig. S2). These findings suggest that the assumption in the VKE approach of a fixed momentum flux is better justified over land than over ocean. Aspects of atmospheric stability seem to play only a marginal role in explaining the bias (*SI Appendix*), and we attribute this difference mostly to the difference in the empirical parameterizations of surface drag over oceans and land that are used in the climate model [and which are commonly used in GCMs (e.g., ref. 24)]. This may relate to a difference in the mechanism by which momentum is transported down to the surface over land and ocean, for instance by differences in boundary layer dynamics or gravity waves (25, 26) This, nevertheless, is likely to have relevant implications, as it suggests that wind power limits may generally be higher over ocean than over land. This aspect would need to be evaluated further.

We thus attribute the bias in VKE to changes in the downward momentum flux, which we correct for by using the GCM simulations (*SI Appendix*, *Supplement B* and Fig. S1). This bias uses separate corrections for ocean and land by empirically relating the surface momentum fluxes of the control climate and the modified surface momentum fluxes of the GCM estimate. The resulting mVKE estimate agrees more closely with the GCM simulations (Figs. 1–3), except for conditions of very high wind speeds like the Southern Ocean, where the decrease in wind speed is underestimated, thus resulting in an overestimation of the wind power limit. For conditions of low to medium wind speeds, the mVKE estimate agrees much better to the GCM estimate (Fig. 2*E*). Overall, the mVKE estimates (global: 0.59 W_e m^{-2}; land: 0.44 W_e m^{-2}; ocean: 0.64 W_e m^{-2})

Table 1. Comparison of wind power limits based on climatology (rows a–l) and GCMs (rows m–z)

Approach for estimation of wind power limit	Global coverage, %	Installed capacity, $MW_i\ km^{-2}$	Wind speed			Electricity generation		
			Control, m s^{-1}	Max. gen., m s^{-1}	Reduced by, %	kWh $m^{-2}\ y^{-1}$	$\sum TW_e$	$W_e\ m^{-2}$
Climatology-based								
Global								
a) VKE (this study)	100	n/a	7.0	4.0	42	2.7	158	0.31
mVKE (this study)	100	n/a	7.0	4.0	42	5.2	302	0.59
b) Gustavson (1979) (18)	100	6.0	—	—	—	2.2	130	0.25
c) Jacobson and Delucchi (2011) (5)	100	—	7.0	—	—	29.2	1,700	3.33
d) Jacobson and Archer (2012) (8)	100	11.3	8.1	—	—	30.0	1,750	3.43
Land								
e) VKE (this study)	26	n/a	4.6	2.7	42	2.8	43	0.32
mVKE (this study)	26	n/a	4.6	2.7	42	3.9	57	0.44
f) Archer and Jacobson (2005) (3)	3.2	9.0	8.4	—	—	37.9	72	4.33
g) Lu et al. (2009) (4)	26	8.9	—	—	—	8.3	126	0.95
h) IPCC (2012) (9), Rogner et al. (2000) (10)	6	n/a	—	—	—	54.7	190	6.24
Oceans								
i) VKE (this study)	71	n/a	7.8	4.5	42	2.5	104	0.29
mVKE (this study)	71	n/a	7.8	4.5	42	5.6	233	0.64
Oceans (nearshore)								
j) Lu et al. (2009) (4)	1.2	5.8	—	—	—	29.4	21	3.36
k) Capps and Zender (2010) (15)	1.2	13.2	9.4	—	—	55.8	40	6.37
Ice								
l) VKE (this study)	3	n/a	8.9	5.1	42	6.3	11	0.72
mVKE (this study)	3	n/a	8.9	5.1	42	6.4	12	0.73
GCM-based								
Global								
m) GCM (this study)	100	10.6	7.0	3.6	48	4.6	270	0.53
n) Jacobson and Archer (2012) (8)	100	11.3	8.1	4.0	51	3.9	224	0.44
o) Marvel et al. (2012) (14)	100	1.7–3.4	9.0	6.3	30	4.8	282	0.55
Land								
p) GCM (this study)	26	24.3	4.6	2.6	44	3.2	49	0.37
q) Miller et al. (2011) (6)	26	15.2	4.3	2.5	42	2.3	34	0.26
r) Jacobson and Archer (2012) (8)	26	11.3	7.5	4.5	40	4.7	71	0.54
s) Wang and Prinn (2010) (19)	11	—	—	—	—	2.9	19	0.33
t) Keith et al. (2004) (11)	2.6	—	—	—	—	10.4	16	1.19
u) Fitch (2015) (20)	0.4	10.0	3.2	2.3	29	5.5	1	0.63
Oceans								
v) GCM (this study)	71	9.1	7.8	3.9	50	5.2	213	0.59
w) Jacobson and Archer (2012) (8)	74	11.3	8.4	4.1	51	3.3	162	0.38
Oceans (nearshore)								
x) Wang and Prinn (2010) (19)	2	—	—	—	—	2.6	3	0.30
y) Wang and Prinn (2011) (21)	2.2	—	—	—	—	5.3	7	0.61
z) Wang and Prinn (2011) (21)	3.6	—	—	—	—	5.6	12	0.64

Estimates by VKE and mVKE are given by rows a, e, i, and l; estimates in rows b and g use long-term global mean near-surface atmospheric dissipation rates as a bound to electricity generation; estimates in rows c, d, f, g, h, j, and k use observed wind speeds and prescribed turbine characteristics without accounting for the reduction in wind speeds. A detailed description of the studies is provided in *SI Appendix, Supplement D*. IPCC, Intergovernmental Panel on Climate Change; Max. gen., maximum electricity generation; n/a, not derived for a specific installed capacity.

compare well with the GCM estimates (global: 0.53 $W_e\ m^{-2}$; land: 0.37 $W_e\ m^{-2}$; ocean: 0.59 $W_e\ m^{-2}$) and are within a factor of 2 over 92% of the nonglaciated land surface and over 93% of the ocean (*SI Appendix*, Fig. S3).

It is important to note that the current state of wind turbine deployment is well below the limits described here. In 2014, the global average generation rate of 0.12 TW_e resulted from a global installed capacity of 0.372 TW_i (1). Assuming only land-based turbines, this generation rate would translate into a wind speed reduction of about 0.05% on land, although this effect may be noticeably higher in some regions with many turbines installed.

The relevance of the reduced wind speeds in the presence of large-scale wind turbine deployments is that this combination results in progressively lower electricity generation by each individual turbine. Each turbine sees a horizontal flux of kinetic energy, $\rho/2\ v^3$ (commonly referred to as wind power density), that, to some extent, is used to generate electricity. With reduced wind speeds, this flux is reduced as well as the per-turbine generation rate and the average capacity factor (which compares the generation rate with what would be generated under optimal conditions). The average capacity factor derived from the GCM simulations is shown in Fig. 4*A*. The decrease in the capacity factor with greater installed capacity directly follows the slowdown of wind speeds and yields a reduction in wind power density according to $(v/v_0)^3$. At maximum wind power use, wind speeds are reduced to 58% of their original value, and lowers the capacity factor to 20% of what would be generated by an isolated turbine. With such a drop of electricity generation per turbine,

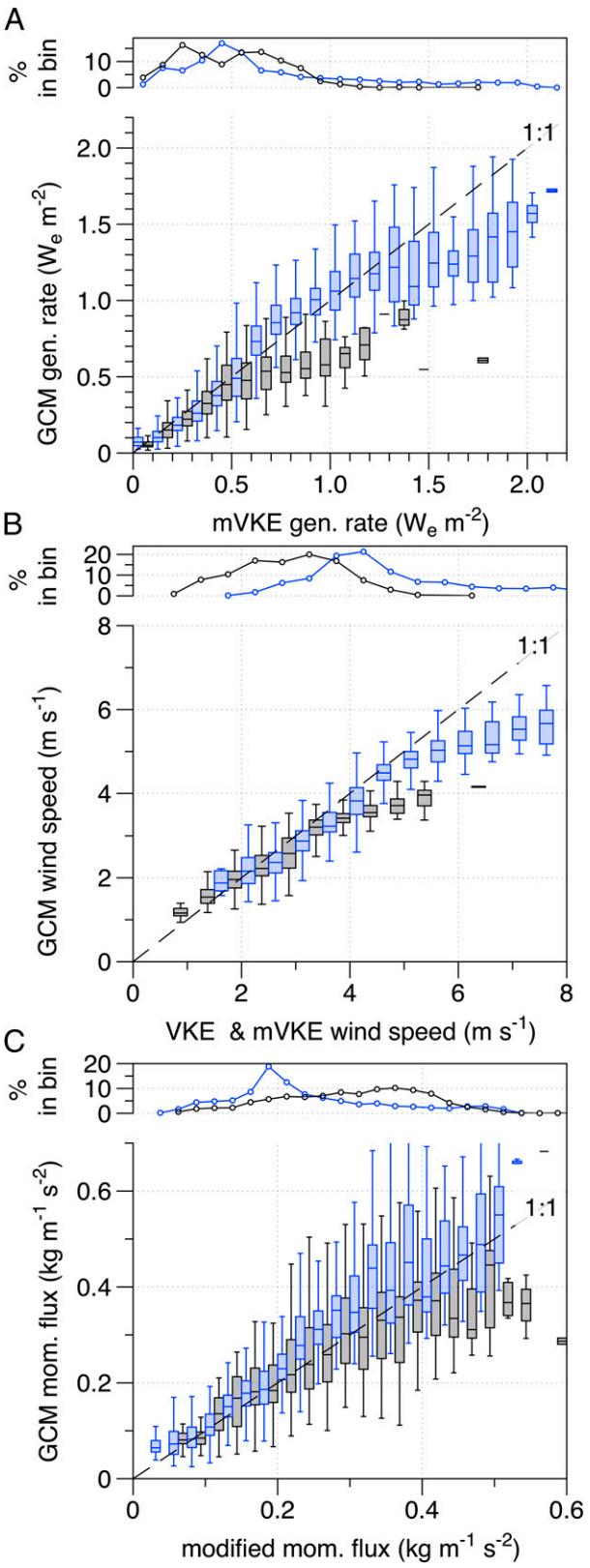

Fig. 3. Grid point comparison of the mVKE estimates to GCM-based estimates at maximum generation for land (black) and ocean (blue) for maximum electricity generation rate (*A*), wind speeds (*B*), and downward momentum flux to the surface (*C*). The top of each plot shows the percentage of data (not area-weighted) within each land or ocean bin. The bin upper and lower bounds are derived from the interquartile range (IQR), with the boxes representing the 25th, 50th, and 75th percentiles. The statistical relationships are provided in *SI Appendix*, *Supplement C*.

wind power is likely to become increasingly more expensive to utilize, so that the limit to wind power use derived here may, in fact, not be economically feasible to achieve. Installed capacities of 5–10 MW_i km^{-2} are common among present-day wind turbine deployments [the US average is about 3 MW_i km^{-2} (0.4–23 MW_i km^{-2}) from 161 operational and planned wind farms (27)], and yet these values are also close to the large-scale limit shown in Fig. 1. This finding suggests that a future increase in the deployment of wind turbines toward larger scales should probably proceed

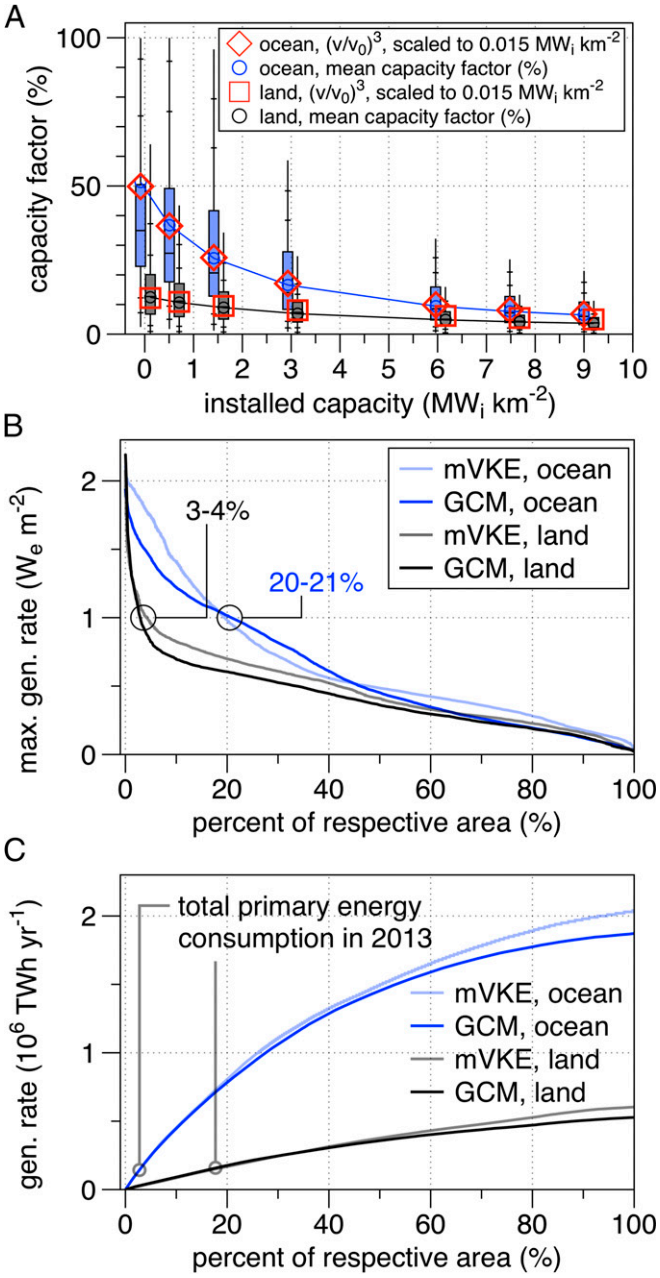

Fig. 4. Comparison of the implications derived from the mVKE and GCM approaches. *A* shows the sensitivity of the capacity factor of individual wind turbines to installed capacity for ocean (blue) and land (black). Also shown by the red symbols is a simple estimate of the capacity factor reduction predicted by the wind speed reduction as $(v/v_0)^3$. *B* shows the distribution of large-scale wind power limits per unit surface area across regions. *C* integrates the distribution shown in *B* to yield estimates for how much area would at a minimum be needed to yield a certain total electricity rate.

at installed capacities well below those currently used to mediate the detrimental effects of reduced wind speeds (also see ref. 28).

The second relevant aspect of these wind power limits is their spatial distribution (Fig. 2). Fig. 4*B* shows the distribution of area according to the wind power limit, showing that the mVKE estimate closely matches the distribution derived from the GCM estimate and that about 3–4% of land and 20–21% of ocean surfaces could, on average, generate more than 1.0 W_e m^{-2}. This electricity generation rate is considerably lower than 0.8–6.6 W_e m^{-2} (with installed capacities of 3.5–24 MW_i km^{-2}) observed from much smaller wind farms operating on hilltops or in coastal arrays (29). When this distribution is integrated over area to derive electricity generation rates (Fig. 4*C*), it indicates that at least 18% of the windiest land areas (or 3% of the windiest ocean areas) would be needed to meet the current primary energy demand of 18 TW. Using lower installed capacities than those associated with the wind power limits, as described above, would imply that a greater area would be needed. Overall, the comparison indicates that the mVKE approach reasonably reproduces these insights from the GCM simulations as well.

Conclusion

We have shown that the large-scale limits to wind power generation can be derived from climatological conditions in a relatively simple and transparent way using the mVKE approach. The mVKE approach uses the momentum balance and accounts for the reduction of wind speeds, as well as how wind turbines can enhance the downward momentum flux to the surface. The resulting wind power limits estimated by mVKE (global: 0.59 W_e m^{-2}; land: 0.44 W_e m^{-2}; ocean: 0.64 W_e m^{-2}) agree well with the GCM estimates (global: 0.53 W_e m^{-2}; land: 0.37 W_e m^{-2}; ocean: 0.59 W_e m^{-2}), with 92% of the land estimates and 93% of the ocean estimates varying within a factor of 2. Because mVKE used only the climatic conditions of the control simulation, this finding suggests that full atmospheric dynamics are not necessarily required to describe atmospheric effects that set the limits to wind power use. The mVKE approach thus represents an approach that can be used with observations to yield more realistic large-scale wind power potentials that account for these critical, atmospheric effects.

We have illustrated that the relevance of this atmospheric perspective on wind power limits goes beyond the number of turbines and their technical specifications. In both the GCM and mVKE approaches, atmospheric effects explicitly shape the wind power limits. As shown in Table 1, there are numerous observation-based approaches that, by neglecting these atmospheric effects, drastically overestimate wind power limits by a factor of 10. Accounting for these atmospheric effects results in large-scale limits to wind power use in most land regions that are well below 1.0 W m^{-2}.

These much lower limits have practical relevance, because reduced wind speeds result in lower average electricity generation rates of each turbine. These lower per-turbine generation rates are also associated with higher generation rates per unit area (W_e m^{-2}) up to the wind power limit, and likely makes wind power less economical at progressively larger deployment scales. Because current values of installed capacity are close to those associated with the limits, this finding implies that the future expansion of wind power should not plan for installed capacities that are much above 0.3 MW_i km^{-2} over areas larger than 10,000 km^2. We conclude that these atmospheric effects need to be considered in actual deployments and future scenarios of wind power at larger scales. Specifically, by understanding the basis of wind power limits and their associated atmospheric effects, we can bound future expansion scenarios by the wind power limit and aim to minimize these atmospheric effects to keep wind power economical and effective in reducing CO_2 emissions, thus counteracting global climate change.

ACKNOWLEDGMENTS. We thank the editor and two anonymous reviewers for their helpful criticisms and suggestions. This study was funded entirely by the Max Planck Society.

1. Wiser R, Bolinger M (2015) 2014 Wind technologies report. *Energy Efficiency and Renewable Energy Report* (US Department of Energy, Washington, DC). Available at energy.gov/sites/prod/files/2015/08/f25/2014-Wind-Technologies-Market-Report-8.7.pdf. Accessed July 4, 2016.
2. International Energy Agency (2013) Renewable energy outlook. *World Energy Outlook 2013*. (International Energy Agency, Paris) Available at www.worldenergyoutlook.org/media/weowebsite/2013/weo2013_ch06_renewables.pdf. Accessed July 4, 2016.
3. Archer C, Jacobson M (2005) Evaluation of global wind power. *J Geophys Res* 110(D12):D12110.
4. Lu X, McElroy MB, Kiviluoma J (2009) Global potential for wind-generated electricity. *Proc Natl Acad Sci USA* 106(27):10933–10938.
5. Jacobson MZ, Delucchi M (2011) Providing all global energy with wind, water, and solar power, Part I: Technologies, energy resources, quantities and areas of infrastructure, and materials. *Energy Policy* 39(3):1154–1169.
6. Miller LM, Gans F, Kleidon A (2011) Estimating maximum global land surface wind power extractability and associated climatic consequences. *Earth Syst Dynam* 2:1–12.
7. Gans F, Miller LM, Kleidon A (2012) The problem of the second wind turbine — a note on common but flawed wind power estimation methods. *Earth Syst Dynam* 3:79–86.
8. Jacobson MZ, Archer CL (2012) Saturation wind power potential and its implications for wind energy. *Proc Natl Acad Sci USA* 109(39):15679–15684.
9. IPCC (2012) *IPCC Special Report on Renewable Energy Sources and Climate Change Mitigation* (Cambridge Univ Press, Cambridge, UK), Chap 7.
10. Rogner H, et al. (2000) Energy resources. *World Energy Assessment. Energy and the Challenge of Sustainability. United Nations Development Programme* (United Nations Department of Economic and Social Affairs, World Energy Council, New York), 508 pp.
11. Keith DW, et al. (2004) The influence of large-scale wind power on global climate. *Proc Natl Acad Sci USA* 101(46):16115–16120.
12. Adams AS, Keith D (2013) Are global wind power resource estimates overstated? *Environ Res Lett* 8:015021.
13. Miller LM, et al. (2015) Two methods for estimating limits to large-scale wind power generation. *Proc Natl Acad Sci USA* 112(36):11169–11174.
14. Marvel K, Kravitz B, Caldeira K (2013) Geophysical limits to global wind power. *Nat Clim Chang* 3:118–121.
15. Capps S, Zender C (2010) Estimated global ocean wind power potential from QuikSCAT observations, accounting for turbine characteristics and siting. *J Geophys Res* 115:D09101.
16. Fraedrich K, Jansen H, Kirk E, Luksch U, Lunkeit F (2005) The planet simulation: Towards a user friendly model. *Meteorol Z* 14:299–304.
17. Lunkeit F, et al. (2007) *Planet Simulator Reference Manual Version 15.0* (Meteorological Institute of the University of Hamburg, Hamburg). Available at https://epic.awi.de/29589/1/Lun2007e.pdf. Accessed July 4, 2016.
18. Gustavson MR (1979) Limits to wind power utilization. *Science* 204(4388):13–17.
19. Wang C, Prinn R (2010) Potential climatic impacts and reliability of very large-scale wind farms. *Atmos Chem Phys* 10:2053–2061.
20. Fitch A (2015) Climate impacts of large-scale wind farms as parameterized in a global climate model. *J Clim* 28:6160–6180.
21. Wang C, Prinn R (2011) Potential climatic impacts and reliability of large-scale offshore wind farms. *Environ Res Lett* 6:025101.
22. Lorenz E (1955) Available potential energy and the maintenance of the general circulation. *Tellus* 7:271–281.
23. Peixoto J, Oort A (1992) *Physics of Climate* (American Institute of Physics, Springer, New York).
24. Polichtchouk I, Shepherd T (August 22, 2016) Zonal-mean circulation response to reduced air-sea momentum roughness. *Q J R Meteorol Soc*, in press.
25. Kirk-Davidoff D, Keith D (2008) On the climate impact of surface roughness anomalies. *J Atmos Sci* 85:2215–2234.
26. Barrie D, Kirk-Davidoff D (2010) Weather response to a large wind turbine array. *Atmos Chem Phys* 10:769–775.
27. Denholm P, Hand M, Jackson M, Ong S (2009) *Land-Use Requirements of Modern Wind Power Plants in the United States* (National Renewable Energy Laboratory, Golden, CO), Tech Rep NREL/TP-6A2-45834.
28. Meneveau C (2012) The top-down model of wind farm boundary layers and its applications. *J Turbul* 13:1–12.
29. MacKay DJ (2013) Could energy-intensive industries be powered by carbon-free electricity? *Philos Trans A Math Phys Eng Sci* 371(1986):20110560.

Supplement A: The GCM approach

We use the PlaSim GCM with a mixed layer ocean and prescribed heat transport, interactive sea ice model, a simple land surface model, and prescribed ice sheets [1,2]. The model is configured at T42 spectral resolution (~2.8º longitude by 2.8º latitude) with 10 atmospheric layers. All simulations are completed for 20 years, with the last 10 years used for analysis. A previous application of this setup showed that it is adequate to reproduce near-surface wind speed statistics [3].

To derive large-scale limits to wind power generation using the GCM, we perform sensitivity simulations using a range of installed capacities (0.02-1360 MW_i km^{-2}). To simulate the deployment of wind turbines near the surface, the drag parameterization for the surface momentum flux (τ) was modified to (as in [3,4]):

(S1) $$\tau = \rho\,(C_n\,|v| + C_{ext}\,|v|) \bullet v$$

where ρ is the air density, C_n is the volumetric drag coefficient for natural turbulence which depends on surface roughness and atmospheric stability, v is the wind speed of the lowest atmospheric level, and C_{ext} is the additional volumetric drag coefficient introduced to simulate momentum transfer by wind turbines. The rate by which turbines extract kinetic energy (P_{ext}) is then given by:

(S2) $$P_{ext} = \rho\,C_{ext}\,v^3$$

A total of 27 simulations with different, globally uniform values for C_{ext} in the range of 10^{-5} to 0.9 were performed. The values of C_{ext} were then converted to the installed capacities of 0.02 to 1360 MW_i km^{-2} using the method described in [5]. Following [6] and [3], we then used a conversion ratio of 2/3 = 66% to relate the spatial and temporal rates of kinetic energy extraction to an electricity generation rate $P_{e,gcm}$ (with the remaining 1/3 being dissipated by wake turbulence):

(S3) $$P_{e,gcm} = 2/3\,\rho\,C_{ext}\,v^3$$

The ratio of 2/3 approximates more complex parameterizations, such as the one used in [11], which iteratively derived this relationship for a specific turbine by explicitly stating the wind speed dependent power coefficients, thrust coefficients, and turbulent kinetic energy coefficients.

Supplement B: The VKE approach

The Vertical Kinetic Energy (VKE) approach [3,5,7] uses the wind speeds (v_0) and surface momentum fluxes (τ_0) from the control simulation of present-day conditions (indicated by the subscript 0) to estimate the large-scale limit to wind power generation. Combining the wind speed and the surface momentum flux yields the downward vertical flux of kinetic energy that maintains wind speeds by continually offsetting turbulent dissipation and that sets the large-scale limit to wind power use. Note that for small wind farms, it is the horizontal flux of kinetic energy ($0.5\ \rho\ v_0^3$) that is the dominant contributor to the electricity generation of small wind farms [8,9]. After the downwind depth of a wind farm exceeds about 10 km, the horizontal influx of kinetic energy has been fully extracted or dissipated [10,3]. As large-scale limits to wind power generation rates are the focus here, the horizontal kinetic energy component can be neglected [10,3], so that it is the vertical downward flux of kinetic energy that sets the upper bound on large-scale wind power generation rate.

In the natural setting without large-scale wind power use, the downward flux of kinetic energy is dissipated by turbulent friction at a rate D_0 given by

(S4) $$D_0 = \tau_0\ v_0$$

As no wind power is extracted, this dissipation rate thus measures the downward flux of kinetic energy to the surface that is potentially available to the wind turbines.

The starting point for VKE is the momentum balance of the lower atmosphere, which is described in steady state by:

(S5) $$0 = J_{m,in} - \tau - F_{ext}$$

with $J_{m,in}$ being the downward flux of horizontal momentum to the surface in the natural state ($J_{m,in} = \tau_0$) and F_{ext} being the drag force of the wind turbines on the atmospheric flow. The momentum flux to the surface is expressed in terms of the common drag formulation, $\tau = \rho\ C_d\ v^2$, with ρ being the air density, C_d the drag coefficent, and v being the wind speed. The momentum balance can be rearranged to yield an expression for how the wind speed changes due to the drag of the turbines:

(S6) $$v = ((J_{m,in} - F_{ext})/(\rho\ C_d))^{1/2}$$

The power extracted by the drag of the wind turbines, P_{ex}, is then given by:

(S7) $$P_{ext} = F_{ext}\ v = F_{ext}\ ((J_{m,in} - F_{ext})/(\rho\ C_d))^{1/2}$$

Note that the extracted power P_{ext} first increases with greater values of the drag F_{ext}, but will then decrease due to the reduction in wind speed. The expression thus has a maximum that can be determined analytically from $\partial P_{ext}/\partial F_{ext} = 0$, which yields optimal expressions associated with the maximum rate by which kinetic energy can be removed by the turbines from the flow:

(S8) $P_{ext,max} = 2/3^{3/2}\ D_0 \approx 0.38\ D_0$
(S9) $F_{ext,opt} = 2/3\ \tau_0$
(S10) $v_{opt} = 1/3^{1/2}\ v_0 \approx 0.58\ v_0$

The extracted power from the flow then contributes to electricity generation and to turbulent dissipation in the turbines' wakes. [6] showed that this partitioning is 2:1 in the ideal case, so that 2/3 of $P_{ext,max}$ represent the limit to electricity generation while 1/3 of $P_{ext,max}$ represent the dissipation by wake turbulence. Hence, the maximum rate of electricity generation associated with wind power in the VKE approach is about 26% of D_0. This formulation of the VKE approach directly follows previous studies [3,5,7].

The VKE estimate of the maximum electricity generation rate ($G_{e,vke}$) is thus given by

(S11) $G_{e,VKE} = 2/3\ (2/3^{3/2}\ \tau_0\ v_0)$

which can be estimated entirely from the atmospheric conditions of the control GCM simulation that includes no effects of wind turbines. We used output of wind speed and surface momentum flux at a high temporal resolution of 3 hours, as variations in v_0 do not average out because $G_{e,vke}$ depends on v_0^3.

To correct for the enhanced downward transport of momentum found in the GCM simulations (Fig. 1, also Fig. S1), we modify the downward momentum flux τ_m as a function of the control value (τ_0). We used separate fits for ocean and land grid points, which are referred to by $\tau_{m,o}$ and $\tau_{m,l}$. The relationship we used over the ocean was:

(S12) $\tau_{m,o} = a \bullet (1-e^{-b\tau_0})$, where a = 0.7 kg m^{-1} s^{-2}, and b = 6 m kg^{-1} s^2

and for land and ice was:

(S13) $\tau_{m,l} = a \bullet (1-e^{-b\tau_0})$, where a = 1.0 kg m^{-1} s^{-2}, and b = 2 m kg^{-1} s^2

These modified momentum fluxes in comparison to the GCM at the maximum generation rate are shown in Fig. S1b. A map of these modified momentum fluxes is shown in Fig. S2c, with a map of the difference between the mVKE and the GCM shown in Fig. S2d.

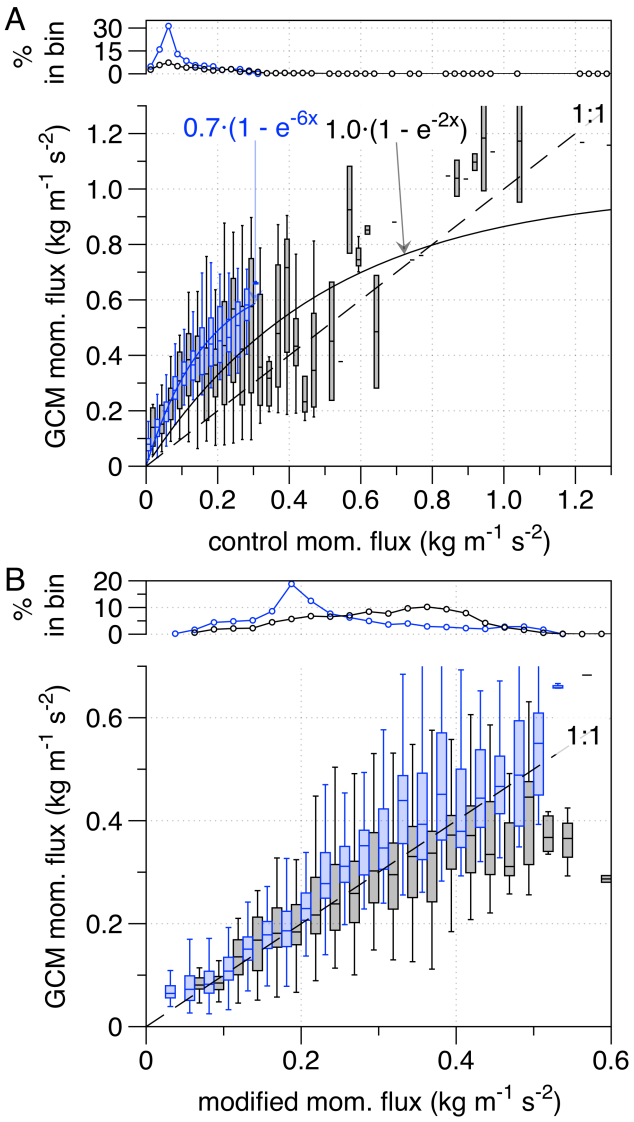

Fig. S1. For land (black) and ocean (blue), **a)** momentum fluxes of the control simulations and GCM at the generation limit, **b)** modified momentum flux (for use in mVKE) derived from applying the equations (S12) and (S13) to the 3-hour control output, compared to the momentum flux of the GCM at maximum generation. The box-whisker plots are binned at 0.025 m^{-1} kg s^{-2} (ocean bins are offset left of center by 0.0125, and land is offset right of center by 0.0125) with the box extent representing the 25-75th percentiles, the box centerline representing the 50th percentile (median) and the extent of the whiskers quantified by the IQR range of each bin. The percent of land or ocean grid points within each bin is shown at the top of each plot.

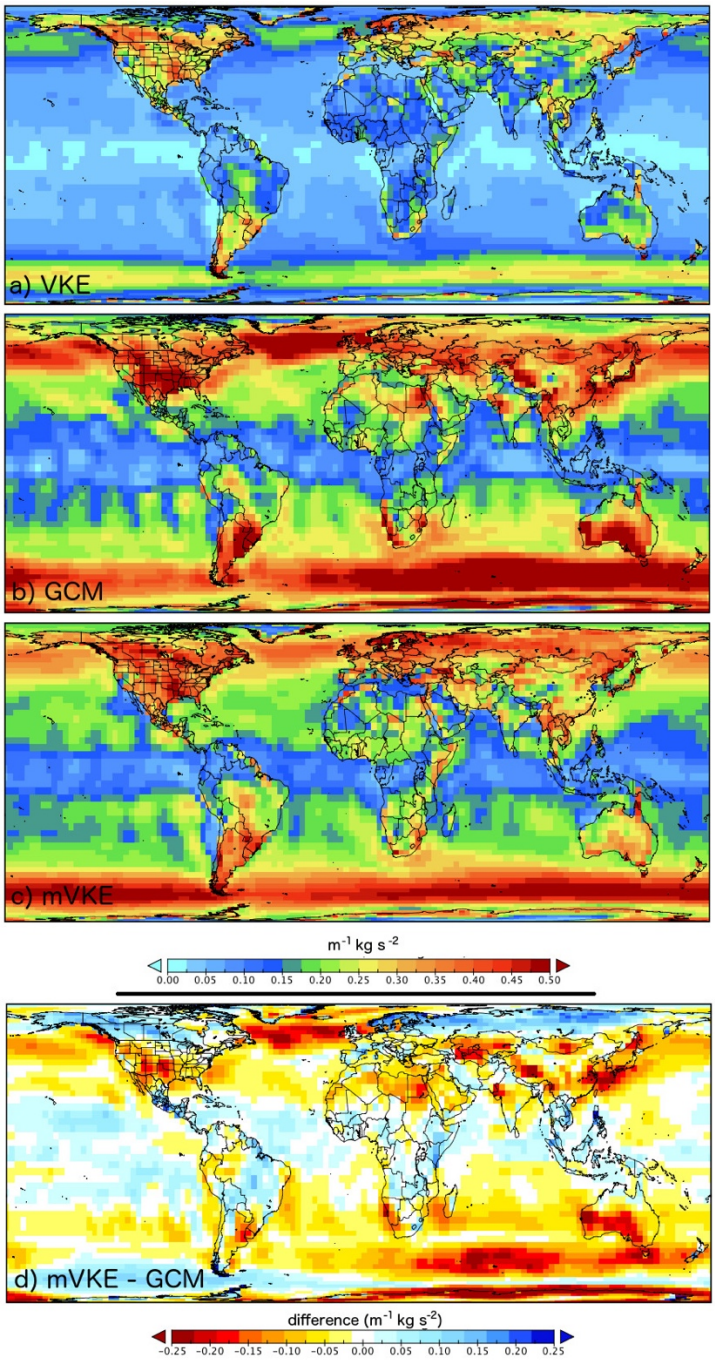

Figure S2. Annual mean surface momentum fluxes **a)** of the control simulation, used in the VKE approach, **b)** at the maximum generation rates of the GCM simulations, **c)** modified by the fits shown in Fig. S1b (Eqs. S12, S13) and used by mVKE, and **d)** differences between the modified momentum flux (c) and the GCM at maximum generation (b).

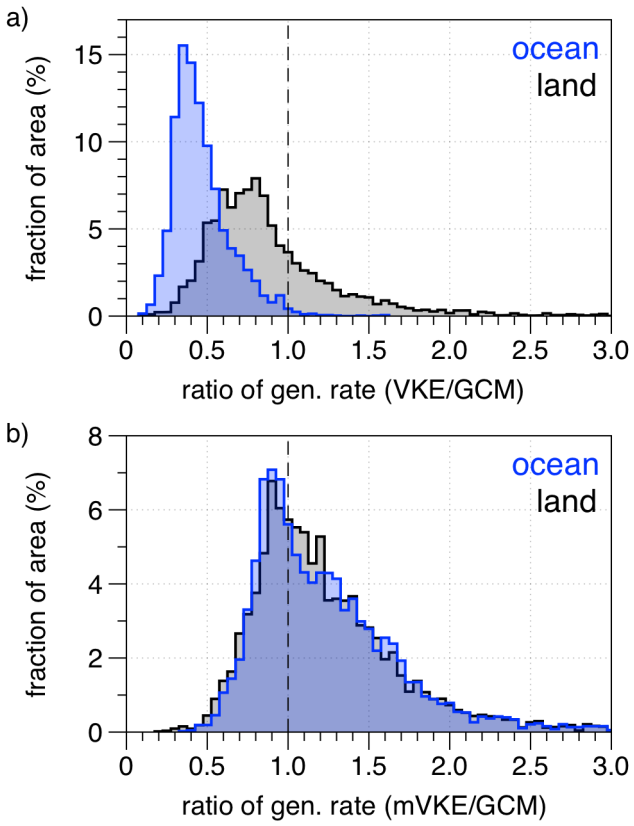

Figure S3. Distribution of how well VKE and mVKE estimates at the grid scale compare to GCM estimates over ocean and land, expressed in terms of the ratios of **a)** VKE/GCM and **b)** mVKE/GCM. A ratio of 1.0 represents perfect agreement. In (a), the generation rates using VKE are within a factor of 2 to the GCM over 87% of the land area and 33% of the ocean area. In (b), the generation rates using mVKE are within a factor of 2 to the GCM over 92% of the land area and 93% of the ocean area.

Supplement C: Extended Information

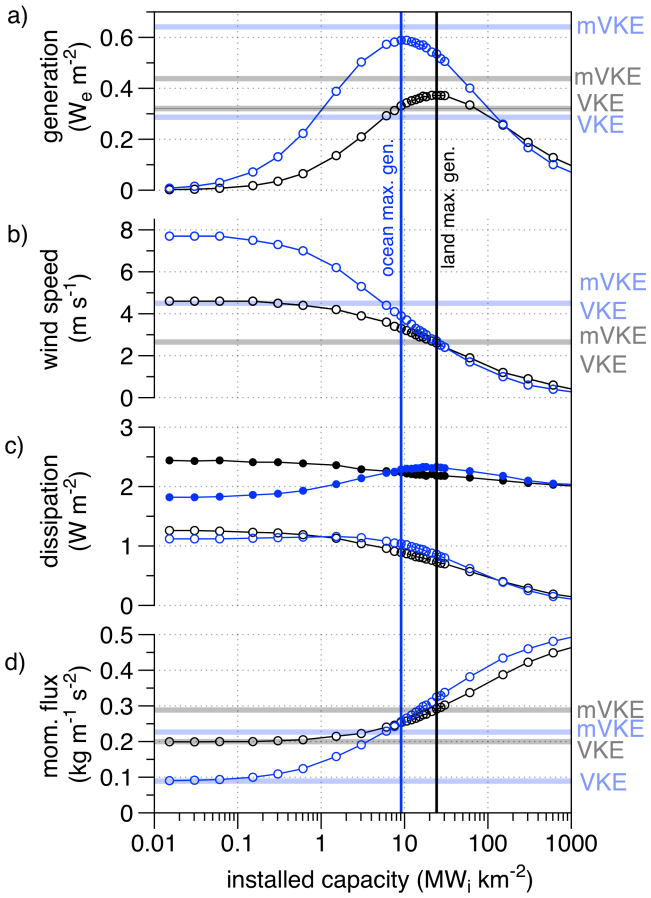

Figure S4. Same as Fig. 1, except this plot shows the entire range of installed capacities simulated with the GCM. With respect to the simulated installed capacity of wind turbines, area-weighted means for ocean (blue) and non-glaciated land (black) for the **a)** rate of electricity generation, **b)** wind speed, **c)** dissipation of the total atmosphere (solid points) and lowest atmospheric level (open points), and **d)** downward flux of horizontal momentum. The vertical lines mark the installed capacities with the respective maximum generation rates over ocean (9 MW_i km^{-2}) or land (24 MW_i km^{-2}). The horizontal lines show the values estimated or used by the VKE and mVKE climatological approaches.

Supplement Table 1: Area-weighted mean values of the range of sensitivity simulations performed in this study for non-glaciated land grid points that are used in Fig. 1, Fig. 4a, and Fig. S4. The gray shaded row is the simulation with the maximum electricity generation rate.

LAND

added drag	installed capacity	generation rate	capacity factor	wind speed	wind speed reduced by	momentum flux to the surface	dissipation rate of the lowest level	dissipation rate of the total atmosphere
-	(MW_i km^{-2})	(W_e m^{-2})	%	(m s^{-1})	(%)	(kg m-1 s^{-2})	(W m^{-2})	(W m^{-2})
0	0.0	0.00	n/a	4.6	0.0	0.20	1.26	2.45
0.00001	0.0	0.00	12.5	4.6	-0.3	0.20	1.26	2.44
0.00002	0.0	0.00	12.3	4.6	0.0	0.20	1.26	2.43
0.00004	0.1	0.01	12.3	4.6	0.3	0.20	1.25	2.44
0.0001	0.2	0.02	11.9	4.6	1.0	0.20	1.23	2.41
0.0002	0.3	0.03	11.5	4.5	2.0	0.20	1.22	2.41
0.0004	0.6	0.06	10.7	4.4	3.8	0.20	1.19	2.39
0.001	1.5	0.14	9.0	4.2	8.4	0.21	1.13	2.36
0.002	3.0	0.21	6.9	3.9	14.3	0.22	1.04	2.29
0.004	6.1	0.29	4.8	3.6	22.4	0.24	0.96	2.26
0.005	7.6	0.31	4.1	3.4	25.9	0.25	0.91	2.24
0.006	9.1	0.33	3.6	3.3	28.3	0.25	0.89	2.24
0.007	10.6	0.34	3.2	3.2	30.6	0.26	0.87	2.22
0.008	12.1	0.35	2.9	3.1	32.9	0.26	0.85	2.21
0.009	13.6	0.36	2.6	3.0	34.8	0.27	0.82	2.20
0.01	15.2	0.36	2.4	2.9	36.5	0.27	0.81	2.20
0.011	16.7	0.37	2.2	2.9	37.8	0.28	0.80	2.20
0.012	18.2	0.37	2.0	2.8	39.5	0.28	0.78	2.18
0.014	21.2	0.37	1.8	2.7	42.0	0.28	0.76	2.21
0.016	24.3	0.37	1.5	2.6	44.2	0.29	0.73	2.18
0.018	27.3	0.37	1.4	2.5	46.2	0.30	0.71	2.18
0.02	30.3	0.37	1.2	2.4	47.9	0.30	0.70	2.18
0.04	60.6	0.33	0.6	1.9	59.6	0.34	0.57	2.15
0.1	151.6	0.26	0.2	1.2	73.2	0.39	0.40	2.10
0.2	303.2	0.19	0.1	0.9	81.5	0.42	0.29	2.06
0.4	606.4	0.13	0.0	0.6	87.8	0.45	0.19	2.03
0.9	1364.4	0.08	0.0	0.3	92.8	0.47	0.12	2.00

Supplement Table 2: Area-weighted mean values of the range of sensitivity simulations performed in this study for ocean grid points that are used in Fig. 1, Fig. 4a, and Fig. S4. The blue shaded row is the simulation with the maximum electricity generation rate.

OCEAN

added drag	installed capacity	generation rate	capacity factor	wind speed	wind speed reduced by	momentum flux to the surface	dissipation rate of the lowest level	dissipation rate of the total atmosphere
-	($MW_i\ km^{-2}$)	($W_e\ m^{-2}$)	%	($m\ s^{-1}$)	(%)	($kg\ m\text{-}1\ s^{-2}$)	($W\ m^{-2}$)	($W\ m^{-2}$)
0	0.0	0.00	n/a	7.8	0.0	0.09	1.12	1.81
0.00001	0.0	0.01	51.33	7.7	0.2	0.09	1.12	1.82
0.00002	0.0	0.02	50.79	7.7	0.4	0.09	1.12	1.82
0.00004	0.1	0.03	49.80	7.7	1.2	0.09	1.12	1.83
0.0001	0.2	0.07	47.18	7.5	2.8	0.10	1.13	1.86
0.0002	0.3	0.13	43.27	7.3	5.5	0.11	1.14	1.88
0.0004	0.6	0.22	36.76	7.0	10.3	0.12	1.15	1.93
0.001	1.5	0.39	25.61	6.2	20.4	0.16	1.16	2.04
0.002	3.0	0.50	16.60	5.3	31.1	0.19	1.14	2.14
0.004	6.1	0.57	9.44	4.4	43.1	0.23	1.08	2.23
0.005	7.6	0.58	7.67	4.1	47.0	0.24	1.05	2.25
0.006	9.1	0.59	6.47	3.9	50.0	0.26	1.04	2.29
0.007	10.6	0.59	5.55	3.7	52.7	0.27	1.02	2.30
0.008	12.1	0.58	4.81	3.5	55.0	0.27	0.99	2.30
0.009	13.6	0.58	4.24	3.3	56.9	0.28	0.97	2.31
0.01	15.2	0.57	3.76	3.2	58.7	0.29	0.95	2.31
0.011	16.7	0.57	3.42	3.1	60.0	0.30	0.94	2.33
0.012	18.2	0.56	3.07	3.0	61.5	0.30	0.91	2.33
0.014	21.2	0.54	2.56	2.8	64.0	0.31	0.88	2.31
0.016	24.3	0.54	2.21	2.7	65.9	0.32	0.86	2.33
0.018	27.3	0.52	1.89	2.5	67.7	0.33	0.82	2.32
0.02	30.3	0.51	1.67	2.4	69.2	0.34	0.80	2.31
0.04	60.6	0.40	0.66	1.7	78.2	0.38	0.62	2.26
0.1	151.6	0.26	0.17	1.0	87.2	0.43	0.39	2.18
0.2	303.2	0.17	0.06	0.6	92.1	0.46	0.25	2.10
0.4	606.4	0.10	0.02	0.4	95.4	0.48	0.15	2.05
0.9	1364.4	0.05	0.00	0.2	97.7	0.50	0.08	2.03

Supplement Table 3: Area-weighted mean values of the range of sensitivity simulations performed in this study for all grid points that are used in Fig. 1, Fig. 4a, and Fig. S4. The light green shaded row is the simulation with the maximum electricity generation rate.

GLOBAL

added drag	installed capacity	generation rate	capacity factor	wind speed	wind speed reduced by	momentum flux to the surface	dissipation rate of the lowest level	dissipation rate of the total atmosphere
-	(MW_i km^{-2})	(W_e m^{-2})	%	(m s^{-1})	(%)	(kg m-1 s^{-2})	(W m^{-2})	(W m^{-2})
0	0.0	0.0000	n/a	7.0	-51.9	0.120	1.19	1.98
0.00001	0.0	0.0062	41.0358	7.0	-51.8	0.121	1.19	1.98
0.00002	0.0	0.0123	40.6334	7.0	-51.4	0.121	1.19	1.98
0.00004	0.1	0.0242	39.8913	6.9	-50.4	0.122	1.19	1.99
0.0001	0.2	0.0574	37.8827	6.8	-48.2	0.123	1.19	2.00
0.0002	0.3	0.1059	34.9276	6.7	-44.7	0.126	1.19	2.01
0.0004	0.6	0.1817	29.9638	6.4	-38.3	0.131	1.18	2.04
0.001	1.5	0.3233	21.3259	5.7	-24.7	0.145	1.18	2.11
0.002	3.0	0.4293	14.1590	5.1	-9.9	0.159	1.13	2.16
0.004	6.1	0.5042	8.3147	4.3	7.2	0.180	1.07	2.21
0.005	7.6	0.5170	6.8206	4.0	12.9	0.187	1.04	2.22
0.006	9.1	0.5269	5.7927	3.8	17.3	0.196	1.02	2.24
0.007	10.6	0.5300	5.0	3.6	21.2	0.201	0.99	2.25
0.008	12.1	0.5284	4.3569	3.5	24.7	0.206	0.97	2.25
0.009	13.6	0.5260	3.8552	3.3	27.6	0.211	0.94	2.25
0.01	15.2	0.5215	3.4400	3.2	30.2	0.215	0.92	2.25
0.011	16.7	0.5235	3.1393	3.1	32.2	0.221	0.92	2.26
0.012	18.2	0.5155	2.8337	3.0	34.6	0.224	0.89	2.25
0.014	21.2	0.5046	2.3775	2.8	38.3	0.230	0.86	2.25
0.016	24.3	0.4990	2.0572	2.7	41.2	0.238	0.84	2.26
0.018	27.3	0.4854	1.7788	2.6	44.1	0.242	0.81	2.24
0.02	30.3	0.4775	1.5749	2.5	46.4	0.248	0.79	2.24
0.04	60.6	0.3919	0.6463	1.8	60.7	0.279	0.62	2.19
0.1	151.6	0.2683	0.1770	1.1	75.8	0.321	0.41	2.12
0.2	303.2	0.1831	0.0604	0.7	84.2	0.346	0.28	2.05
0.4	606.4	0.1177	0.0194	0.5	90.2	0.367	0.18	2.01
0.9	1364.4	0.0661	0.0048	0.2	94.6	0.386	0.10	1.98

Statistics related to Fig. 3

These statistical relationships of Figure 3 are not area-weighted. GCM and mVKE values are given for both land and ocean, comprising 1859 values on land (no ice) and 5426 over ocean.

In Fig. 3a, comparing the mVKE generation rate to the GCM-based maximum generation rates over land to the maximum generation rate by mVKE: land mean GCM=0.40 W_e m^{-2}, land mean mVKE=0.49 W_e m^{-2}, land standard deviation of GCM= 0.20 W_e m^{-2}, land standard deviation of mVKE= 0.25 W_e m^{-2}, standard error of the means=0.0036, mean absolute error=0.13, root mean square error=0.18, and based on Welch's 2-sample t-test, t=12.28, p-value < 2.2e-16, and the 95th confidence intervals of 0.077 and 0.106. For the ocean: ocean mean GCM=0.65 W_e m^{-2}, ocean mean mVKE=0.71 W_e m^{-2}, ocean standard deviation of GCM= 0.43 W_e m^{-2}, ocean standard deviation of mVKE= 0.47 W_e m^{-2}, standard error of the means=0.0027, mean absolute error=0.15, root mean square error=0.21, and based on Welch's 2-sample t-test, t=6.628, p-value = 3.7e-11, and the 95th confidence intervals of 0.04 to 0.07.

In Fig. 3b, comparing the wind speed at maximum generation estimated by VKE and mVKE (equivalent to 57.7% of the control wind speed) to the GCM at maximum generation: land mean GCM=2.75 m s^{-1}, land mean mVKE=2.87 m^{-1} s^{-1}, land standard deviation GCM=0.73 m^{-1} s^{-1}, land standard deviation mVKE=0.93 m^{-1} s^{-1}, standard error of the mean=0.0099, mean absolute error=0.349, root mean square error=0.444, and based on Welch's 2-sample t-test, t=4.50, p-value =7.0e-6, and the 95th confidence intervals of 0.0696 and 0.1771. For ocean, ocean mean GCM=4.04 m^{-1} s^{-1}, ocean mean mVKE=4.68 m^{-1} s^{-1}, ocean standard deviation GCM=1.05 m^{-1} s^{-1}, ocean standard deviation mVKE=1.40 m^{-1} s^{-1}, standard error of the mean=0.0086, mean absolute error=0.687, root mean square error=0.906, and based on Welch's 2-sample t-test, t=-27.043, p-value <2.2e-16, and the 95th confidence intervals of 0.597 to 0.691.

In Fig. 3c, comparing the modified momentum flux used by mVKE to the GCM at maximum generation: land mean GCM=0.29 m^{-1} kg s^{-2}, land mean VKE=0.30 m^{-1} kg s^{-2}, land standard deviation GCM=0.11 m^{-1} kg s^{-2}, land standard deviation mVKE=0.10 m^{-1} kg s^{-2}, standard error of the mean=0.0021, mean absolute error=0.07, root mean square error=0.09, and based on Welch's 2-sample t-test, t=3.02, p-value =0.00251, and the 95th confidence intervals of 0.0037 and 0.0171. For the ocean, ocean mean GCM=0.27 m^{-1} kg s^{-2}, ocean mean mVKE=0.24 m^{-1} kg s^{-2}, ocean standard deviation of GCM=0.14 m^{-1} kg s^{-2}, ocean standard deviation of mVKE=0.11 m^{-1} kg s^{-2},, standard error of the mean=0.00097, mean absolute error=0.055, root mean square error=0.077, and based on Welch's 2-sample t-test, t=12.43, p-value <2.2e-16, and the 95th confidence intervals of -0.0344 to -0.0250.

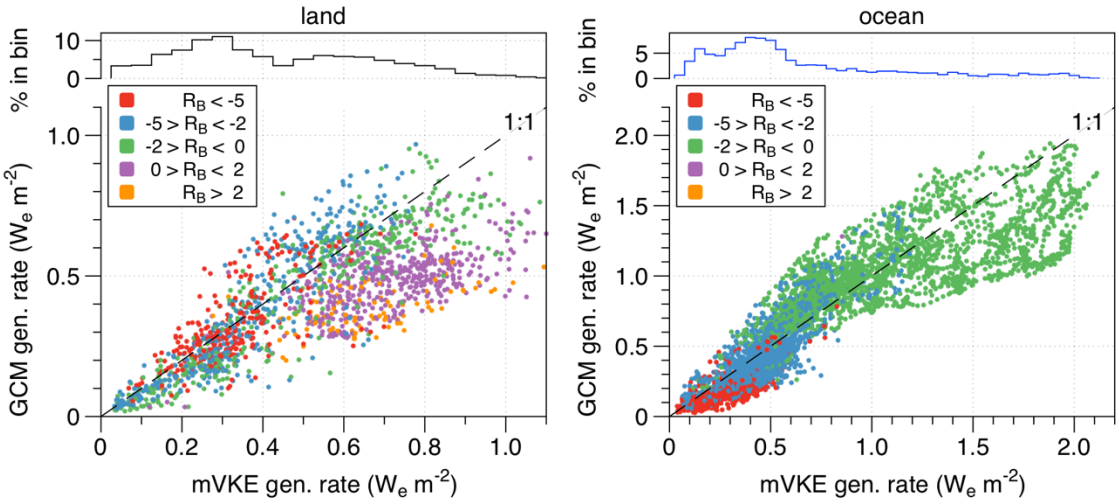

Figure S5. 10-year mean generation rate estimated by the modified VKE (mVKE) approach compared to the GCM simulations at maximum generation (land=24 MW_i km^{-2}, ocean=9.1 MW_i km^{-2}), with the colors shaded according to the bulk Richardson values of the control simulation. The histograms at the top of each plot are grid-area weighted to the percent of the mVKE estimate within each bin.

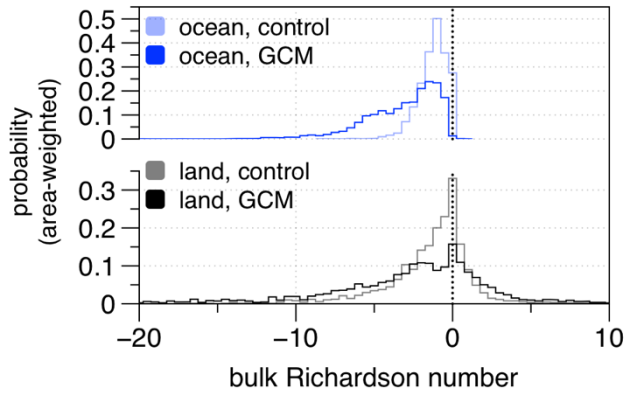

Figure S6. 10-year mean bulk Richardson values over the ocean (blue) and land (black) for the control simulation and GCM simulation at maximum generation.

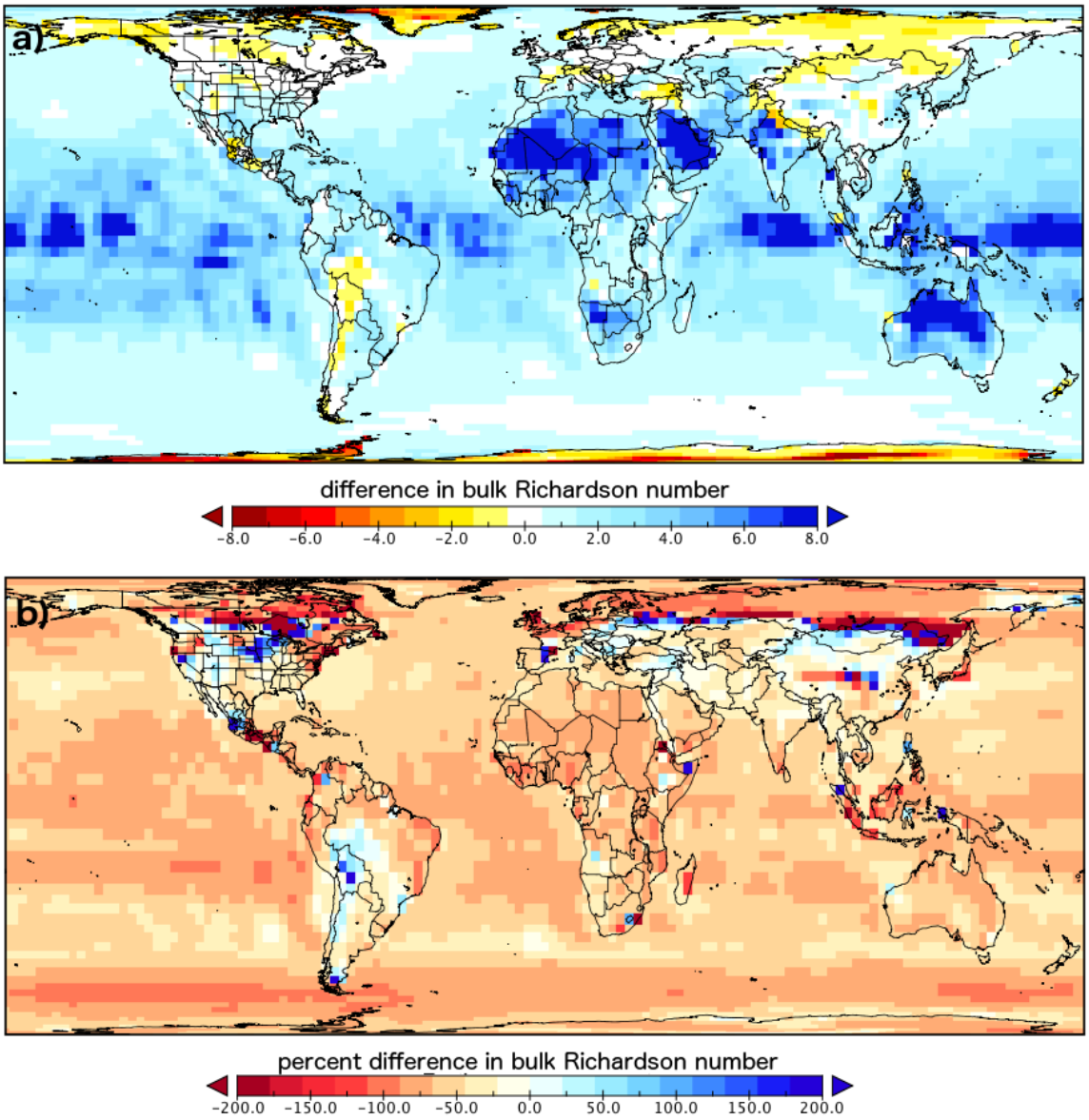

Figure S7. **a)** Difference between the bulk Richardson numbers at the maximum respective ocean and land generation rates of the GCM, compared to the pre-turbine control, *i.e.* GCM-control, **b)** Percent difference between the bulk Richardson values at the maximum respective ocean and land generation rates of the GCM, compared to the pre-turbine control, *i.e.* (GCM-control)/control • 100.

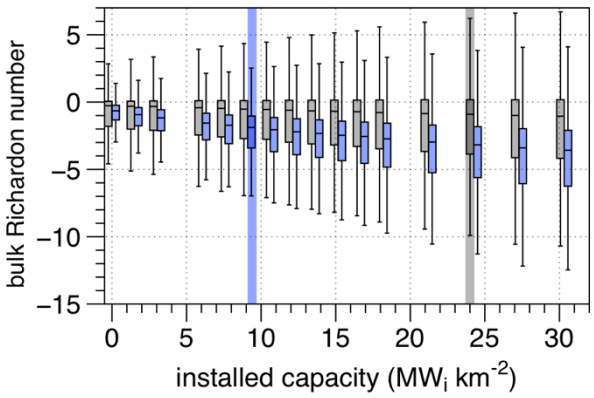

Figure S8. 10-year mean bulk Richardson number for each land (black) and ocean (blue) grid point, with the interquantile range in values shown by the extent of each bar and the boxes indicating the 25th, 50th, and 75th percentiles

Supplement D: Extended details of Table 1

The values stated in Table 1 are often dispersed throughout the referenced text and supplements, and in a few cases, not stated explicitly. This section provides the details for how the referenced entries of Table 1 were derived.

(a) VKE (this study) – Global - Climatology based

The values in Table 1 are derived in this study. They represent a case of 100% global coverage by wind turbines, use a mean pre-turbine wind speed of 7.0 m s^{-1} of the GCM control climate, a wind speed of 4.0 m s^{-1} at maximum generation (reduced by 42%). The momentum flux to the surface (0.120 kg m^{-1} s^{-2}) is also used. This combination of wind speed reduction and control momentum flux to the surface yields a maximum mean electricity generation rate of 0.31 W_e m^{-2} corresponding to 2.7 kWh m^{-2} yr^{-1} or a mean rate of 158 TW_e.

mVKE (this study) – Global - Climatology based

The values in Table 1 are derived in this study. They represent a case of 100% global coverage by wind turbines, use a mean pre-turbine wind speed of 7.0 m s^{-1} of the GCM control climate, a wind speed of 4.0 m s^{-1} at maximum generation (reduced by 42%). Based on the steps described in Supplement A, the area-weighted modified momentum flux used in mVKE at the global scale is 0.24 kg m^{-1} s^{-2}. This combination of wind speed reduction and modified momentum flux to the surface yields a maximum mean electricity generation rate of 0.59 W_e m^{-2} corresponding to 5.2 kWh m^{-2} yr^{-1} or a mean rate of 302 TW_e.

(b) [11] – Global - Climatology based

The values in Table 1 for Gustavson (1979) represent 100% global coverage, a maximum generation rate from an installed capacity of 6.0 MW_i km^{-2}, a maximum generation rate of 0.25 W_e m^{-2} which corresponds to 2.2 kWh m^{-2} yr^{-1} or 130 TW_e.
In Gustavson (1979) Table 1, the maximum generation rate is given as 0.25 $W_e m^{-2}$, or 130 TW_e globally and 2.0 TW_e for the lower 48 contiguous states of the United States. This generation rate estimate is derived by assuming that a maximum of 10% of the near-surface dissipation is extracted. This 10% reflects, "…a compromise between caution and imprudence in the face of inadequate knowledge, 10 percent of the near-surface dissipation will be taken here as a limiting value," (p.14).

The calculation of the installed capacity is not provided in Gustavson's Table 1. We derived it here by back-calculating it from the spacing parameter (λ) for the United States estimate, where λ=0.02. This spacing parameter corresponds to the "…ratio of the rotor-swept area to the land surface area," (Gustavson, p.15). Consistent with the age of this publication, we chose the technical specifications of the Vestas V60, with its rated capacity (*i.e.* maximum generation rate per turbine) of 850 kW_e and 60-meter rotor diameter. This yields an installed capacity of 6.02 MW_i km^{-2}. As a crosscheck to more recent wind turbines, we substitute the technical specifications of the Vestas V112, with its rated capacity of 3.075 MW_e and 112-meter rotor diameter, which yields an installed capacity of 6.24 MW_i km^{-2}. Given these similar estimates, we used a value of 6.0 MW_i km^{-2}.

(c) [12] – Global - Climatology based

This study dealt with a case of 100% global coverage by wind turbines, used a pre-turbine wind speed of 7.0 m s^{-1} at hub-height, derived a mean electricity generation rate of 3.33 W_e m^{-2}, which corresponds to 29.2 kWh m^{-2} yr^{-1} or 1700 TW_e.

Jacobson & Delucchi (2011) Table 3 states the power available worldwide from wind as 1700 TW, which accounts for all wind speeds at 100 meters over land and ocean. Using the global surface area of $5.1 \cdot 10^{14}$ m^2 allows one to derive the mean electricity generation rate per unit area as 3.33 W_e m^{-2} (or 29.2 kWh m^{-2} yr^{-1}). Jacobson & Delucchi (2011) Fig. 1 shows global winds speeds at 100 meters with a mean of 7.0 m s^{-1} (land=6.1 m s^{-1}, ocean=7.3 m s^{-1}).

(d) [13] – Global - Climatology based

Jacobson & Archer (2012) considered a case of 100% global coverage by wind turbines, a maximum generation rate from an installed capacity of 11.3 MW_i km^{-2}, pre-turbine wind speed of 8.1 m s^{-1} at hub-height, with a maximum generation rate of 3.43 W_e m^{-2} which corresponds to 30.0 kWh m^{-2} yr^{-1} or 1750 TW_e.

This wind power generation limit is quite similar to the above-noted global estimate of 1700 TW_e by Jacobson & Delucchi (2011), but Jacobson & Archer (2012) provide more details on the methodology. The revised generation rate of 1750 TW_e assumes an installed capacity of 11.3 MW_i km^{-2}, but considers "…no momentum extraction from them [the turbines]," p.15680.

In Table 1 of Jacobson & Archer (2012) values are shown in which wind turbines interact with the atmosphere and with each other. This interaction reduces the estimated global generation rate from 1750 TW_e to 224 TW_e (see also rows m, q, and v in Table 1).

(e) VKE (this study) – Land - Climatology based

The values are taken from this study. Covering land regions without permanent ice cover with wind turbines represent a case of 26% global coverage. The mean pre-turbine wind speed of 4.6 m s^{-1} is used (cf. Fig. 1) with a mean wind speed of 2.7 m s^{-1} at maximum generation (reduced by 42%), generating a mean of 0.32 W_e m^{-2} of electricity, corresponding to 2.8 kWh m^{-2} yr^{-1} or 43 TW_e.

mVKE (this study) – Land - Climatology based

The values in Table 1 are derived in this study. Covering land regions without permanent ice cover with wind turbines represent a case of 26% global coverage. The mean pre-turbine wind speed of 4.6 m s^{-1} is used (cf. Fig. 1) with a mean wind speed of 2.7 m s^{-1} at maximum generation (reduced by 42%). Based on the steps described in Supplement A, the area-weighted modified momentum flux used in mVKE is 0.29 kg m^{-1} s^{-2}. This combination of wind speed reduction and modified momentum flux to the surface yields a maximum mean electricity generation rate of 0.44 W_e m^{-2} corresponding to 3.9 kWh m^{-2} yr^{-1} or a mean rate of 57 TW_e.

(f) [14] – Land – Climatology based

Table 1 lists for this study a global coverage of 3.2%, an installed capacity of 9.0 MW_i km^{-2}, a pre-turbine wind speed of 8.4 m s^{-1} at hub-height, and a mean electricity generation rate of 4.33 W_e m^{-2} which corresponds to 37.9 kWh m^{-2} yr^{-1} or 72 TW_e.

Archer & Jacobson (2005) used observations from year 2000. From all stations that they consider (which include Surface Stations and Sounding Stations), their Table 1 lists 12.7% of stations that are wind class 3 or better (≥6.9 m s^{-1} at 80-meter hub-height). From their Table 4, the mean 80-meter wind speed at these stations is 8.40 m s^{-1} over land, and 8.44 m s^{-1} for all stations. For the non-glaciated land area a value of $1.3 \cdot 10^{14}$ m^2 is used (paragraph 53). Paragraph 56 states that 6 turbines of 1.5 MW_i capacity are used per square kilometer (corresponding to a spacing of 4 rotor diameters x 7 rotor diameters), and therefore correspond to an installed capacity of 9.0 MW_i km^{-2}. The wind power generation rate is then estimated as 71.5 TW_e in paragraph 57 for a generation rate per unit surface area of 4.33 W_e m^{-2} which corresponds to 37.9 kWh m^{-2} yr^{-1}.

(g) [15] – Land – Climatology based

Table 1 lists a global coverage of 26% for this study, an installed capacity of 8.9 MW_i km^{-2}, a mean electricity generation rate of 0.95 W_e m^{-2} which corresponds to 8.3 kWh m^{-2} yr^{-1} or 126 TW_e.

The percent of global coverage was difficult to deduce from the methods in Lu et al. (2009). Using a MODIS land cover classification for 2001, the following areas were excluded from wind power deployment: forest, permanent snow and ice, water, and areas classified as developed or urban. Visually referencing these areas from the Figure 1 map of Lu et al. (2009), the following non-glaciated land regions were excluded: a stripe across Scandinavia and through the Russian Federation, a large fraction of the forested area of South America, and a large fraction of forested area in the Democratic Republic of the Congo. Assuming the control wind speeds of our GCM (Fig. 1b) are consistent with the wind speeds used by Lu et al. (2009), the equatorial forests have low wind speeds over large spatial areas, suggesting their exclusion would increase the mean area-weighted generation rate on land. The influence of excluding the band across Scandinavia and Russia is less clear, as according to Fig. 1 of Lu et al. (2009), this region is bound by wind power generation rates of 1-3 W_e m^{-2}. With caution, we assumed a deployment area on land of 26%, which is consistent with several of the other studies used in Table 1 (*i.e.* Miller et al., 2011, Jacobson & Archer, 2012).

The installed capacity is noted as one 2.5 MW_i turbine for each 0.28 km^2, yielding an installed capacity of 8.9 MW_i km^{-2}. Table 2 of Lu et al. (2009) states the annual wind energy generation rate is 1100 PWh, excluding any further spatial restrictions (such as low per-turbine generation rates from deploying wind turbines in 'calm' regions). We converted the PWh value to a mean generation rate of 125.6 TW_e per year. Combining this generation rate with the assumed onshore area of ~$1.326 \cdot 10^{14}$ m^2 (26% of global surface area) yields a mean generation rate 0.95 W_e m^{-2}.

(h) [16] – Land – Climatology based

Table 1 lists a global coverage of 6% for this study, a mean electricity generation rate of 6.24 W_e m^{-2} which corresponds to 54.7 kWh m^{-2} yr^{-1} or 190 TW_e.

The IPCC (2012) states in the Wind Energy Section, Resource Potential, Sec. 7.2, of the Special Report on Renewable Energy Sources and Climate Change Mitigation (SRREN), on p.543 "*The theoretical potential for wind, as estimated by the global annual flux, has been estimated at 6,000 EJ/yr (Rogner et al., 2000)*."

On p.964, the theoretical potential is defined as follows: "*Theoretical potential is derived from natural and climatic (physical) parameters (e.g., total solar irradiation on a continent's surface). The theoretical potential can be quantified with reasonable accuracy, but the information is of limited practical relevance. It represents the upper limit of what can be produced from an energy resource based on physical principles and current scientific knowledge. It does not take into account energy losses during the conversion process necessary to make use of the resource, nor any kind of barriers.*"

Our interpretation of "*The theoretical potential for wind, as estimated by the global annual flux, has been estimated at 6,000 EJ/yr (Rogner et al., 2000)"* is that this is a global theoretical potential for wind, however Table 5.20 on p.164 of [17] describes this estimate as representing something quite different. The "*Assessed wind energy potential*" of 6000 EJ/yr is derived from the windiest land areas, "*with average annual power density of more than 250-300 watts per square metre at 50 metres.",* which according to the same Table 5.20 represents 23% of land area. We therefore interpreted these numbers as described in the original source [17].

The area would therefore be 23% (windy land) of about 26% of the global surface that is land, or approximately 6% of the global surface ($3.0 \cdot 10^{13}$ m^2) for 190.3 TW_e (6000 EJ/yr) of theoretical potential. Specific to these windiest land areas, this is 6.24 W_e m^{-2} which corresponds to 54.7 kWh m^{-2} yr^{-1}.

(i) VKE (this study) – Ocean - Climatology based

The values are taken from this study. They are represented by a global coverage of 71%, a mean pre-turbine wind speed of 7.8 m s^{-1}, a wind speed at maximum generation of 4.5 m s^{-1} (reduced by 42%), and a maximum electricity generation rate of 0.29 W_e m^{-2}, which corresponds to 2.5 kWh m^{-2} yr^{-1} or 104 TW_e.

mVKE (this study) – Ocean - Climatology based

The values in Table 1 are derived in this study. They are represented by a global coverage of 71%, a mean pre-turbine wind speed of 7.8 m s^{-1}, a wind speed at maximum generation of 4.5 m s^{-1} (reduced by 42%).

Based on the steps described in Supplement A, the area-weighted modified momentum flux used in mVKE is 0.23 kg m^{-1} s^{-2}. This combination of wind speed reduction and modified momentum flux to the surface yields a maximum mean electricity generation rate of 0.64 W_e m^{-2} corresponding to 5.6 kWh m^{-2} yr^{-1} or a mean rate of 233 TW_e.

(j) [15]]

For this study, Table 1 lists a global coverage of 1.2% with an installed capacity of 5.8 MW_i km^{-2}, a mean electricity generation rate of 3.36 W_e m^{-2}, which corresponds to 29.4 kWh m^{-2} yr^{-1} or 21 TW_e.

The percent of global coverage was not stated in the paper. Lu et al. (2009) used a bathymetric threshold of ≤ 200-meters with an added specification of being within 50

nautical miles (92.6 km) of a shoreline. This region is similar to Capps & Zender (2010), except that [18] also used a minimum wind speed threshold. According to Table 2 of Lu et al. (2009), the offshore wind power generation rate used a case where deployed turbines exceed a 20% capacity factor (i.e., the 3.6 MW_i turbine is estimated to achieve a mean generation rate of 0.72 MW_e). This case yields 157 PWh yr^{-1} (or 17.92 TW_e), while the contribution of additional wind turbines deployed in less windy regions increases the generation rate to 180 PWh yr^{-1} (20.55 TW_e).

With caution, we will therefore use the 1.2% global coverage of [18] as being representative of the deployed nearshore ocean of Lu et al. (2009). This yields mean generation rates of 2.93 and 3.36 W_e m^{-2} for the two different generation rates from Lu et al. (2009) Table 2. Given the intention of our study's Table 1 to document the maximum limit to generation rate, we therefore used the generation rate of 3.36 W_e m^{-2}.

(k) [18]

Table 1 uses values of 1.2% global coverage, an installed capacity of 13.2 MW_i km^{-2}, a mean pre-turbine wind speed of 9.43 m s^{-1} at hub-height, and a mean electricity generation rate of 6.37 W_e m^{-2}, which corresponds to 55.8 kWh m^{-2} yr^{-1} or 39.8 TW_e.

Case 3 listed in Table 3 in Capps & Zender (2010) states that the ocean region with a mean wind speed ≥ 7.1 m s^{-1} at 100-meter hub-height and a maximum water depth of 200-meters encompasses an area of $6.25 \cdot 10^{12}$ m^2. Using a global surface area of $5.1 \cdot 10^{14}$, this corresponds to a global coverage of 1.2%. Case 3 in Table 3 also lists a mean wind speed at the 100-meter hub-height for this region as 9.43 m s^{-1}. From their Table 4, the maximum generation rate for Case 3 was estimated using the Vestas V90 3.0 MW_i turbine, yielding 39.8 TW_e from a turbine-spacing of 4 rotor diameters by 7 rotor diameters. Using this generation rate for the covered area yields a mean generation rate per unit area of 6.37 W_e m^{-2} or 55.8 kWh m^{-2} yr^{-1}. The turbine density for Case 3 in Table 4 is listed as 4.41 turbines of 3.0 MW_i capacity per square kilometer, which yields an installed capacity of 13.2 MW_i km^{-2}.

(l) VKE (this study) – Ice - Climatology based

The values are taken from this study. The regions covered by permanent ice correspond to a global coverage of 3%. Over these regions, the mean pre-turbine wind speed is 8.9 m s^{-1}, a wind speed of 5.1 m s^{-1} at maximum generation (reduced by 42%), yielding a mean electricity generation rate of 0.72 W_e m^{-2}, which corresponds to 6.3 kWh m^{-2} yr^{-1} or 11 TW_e.

(m) GCM (this study) – Global – Climate model based

The values are taken from this study. They represent 100% global coverage, use a mean pre-turbine wind speed of 7.0 m s^{-1}, a wind speed of 3.6 m s^{-1} at maximum generation (reduced by 48%) at an installed capacity of 10.6 MW_i km^{-2}, yielding a mean electricity generation rate of 0.53 W_e m^{-2}, which corresponds to 4.6 kWh m^{-2} yr^{-1} or 270 TW_e.

Supplement Table 3 shows the global area-weighted values for all simulations.

(n) [13] – Global – Climate model based

The study by Jacobson & Archer (2012) corresponds to 100% global coverage, derived a maximum generation rate from an installed capacity of 11.3 MW_i km^{-2}, used a mean pre-turbine wind speed of 8.1 m s^{-1} at hub-height, a mean wind speed of 4.0 m s^{-1} at hub-height at maximum generation (reduced by 51%), with a maximum electricity generation rate of 0.44 W_e m^{-2}, which corresponds to 3.9 kWh m^{-2} yr^{-1} or 224 TW_e. Note that a slightly higher global generation rate of 253 TW_e is also stated in Jacobson & Archer (2012) for a short simulation with higher resolution, although less information is provided for this simulation.

Jacobson & Archer (2012) show in Fig S3A in their supplementary information the mean pre-turbine wind speeds at a 100-meter hub-height, with the global mean wind speed stated as 8.13 m s^{-1}. This is denoted as their control. Their control simulation (Simulation A) also includes wind turbines with an installed capacity of 11.3 MW_i km^{-2} and a hub-height of 100 meters, "…but no momentum extraction from them" (p.15680) yielding a mean global generation rate of 1750 TW_e (3.43 W_e m^{-2}).

By including the effect of the wind turbines on the atmospheric flow (their Simulation B), the same global installed capacity of 11.3 MW_i km^{-2} generated 224 TW_e (0.44 W_e m^{-2}). They also list a Simulation C in their Table 1, which yielded a slightly higher global mean generation rate of 228 TW_e (0.44 W_e m^{-2}) and was then used to upscale the generation rates resulting from higher horizontal simulations (Simulation G with a resolution of 2ºx2.5º and Simulation H with a 1.5ºx1.5º resolution) calculated over shorter time periods (one year for G and six months for H respectively). With respect to wind speed reductions, the supplementary information only describes the mean and spatial differences in wind speed in comparing not Simulation C, but rather Simulation B (224 TWe from an installed capacity of 11.3 MW_i km^{-2}) to the control simulation. As shown in Fig. S3Bii of their supplementary information, the global mean wind speed at the 100-meter hub-height for Simulation B has been reduced to 4.0 m s^{-1}(reduced by 51%).

(o) [19] – Global – Climate model based

The study of Marvel et al. (2012) considered a 100% global coverage by wind turbines, lists a mean pre-turbine wind speed of 9.0 m s^{-1}, a wind speed of 6.3 m s^{-1} at maximum generation (reduced by 30%), generating electricity at a mean rate of 0.55 W_e m^{-2}, which corresponds to 4.8 kWh m^{-2} yr^{-1} or 282 TW_e.

Marvel et al. (2012) do not calculate a generation rate, but rather the atmospheric kinetic energy extraction rate resulting from a sensitivity of added momentum sinks. According to Figure 1a of Marvel et al. (2012), an effective area of added drag of 10000 m^2 km^{-3} to the lowest two atmospheric levels of the global climate model yields a kinetic energy extraction rate of 428 TW. Corten (2001) describes that from this extraction rate, a maximum of 2/3 could be converted to electricity, the same factor that we used in our methodology. This same conversion factor of 2/3 yields a mean electricity generation rate per unit area of 0.55 W_e m^{-2} or 282 TW_e globally.

Figure 1a in Marvel et al. (2012) shows that kinetic energy extraction rates (and thereby generation rates) in their simulations increase up to the highest modeled momentum sink (10 000 m^2 km^{-3}). To relate their y-axis of Figure 1a ("Density of effective area of added drag (m^2 km^{-3})") to wind turbine installed capacity (in units of MW_i km^{-2}) used in other studies (including this study), we need to convert their effective area to the cross section of wind turbines. Marvel et al. (2012) introduced

an additional momentum sink term to the lowest 2 of 26 vertical levels. Assuming the total height of these lowest 2 model levels is about 250 m, the effective area of added drag for 10 000 m^2 km^{-3} is roughly 250m x 1000m x 1000m x $10^4 m^2/10^9 m^3$ = 2500 m^2. By instead using a height of 500-meters, the effective drag area increases to 5000 m^2. The 2 MW_i Tjaereborg wind turbine used in our study has a rotor diameter of 61-meters, with a rotor-swept area of 2922 m^2. This allows us to relate the "Density of effective area of added drag" in Marvel et al. (2012) to an installed capacity of about 1.7-3.4 MW_i km^{-2}. Figure A1(b) of Marvel et al. (2012) shows that the "Global Average Near-Surface Wind Speed (m/s)" decreases from about 9 m s^{-1} to about 6.3 m s^{-1} (a reduction by 30%) at the above-noted maximum.

The above-noted assumptions applied to Marvel et al. (2012) allows its comparison to other large-scale climate modeling studies, with an installed capacity of 1.7-3.4 MW_i km^{-2} generating about 0.55 W_e m^{-2} while being associated with a reduction in mean wind speeds by about 30%. From our own simulations as shown in Supplement Table 3 (*i.e.* global area-weighted mean values), an installed capacity of 3.0 MW_i km^{-2} generates 0.43 W_e m^{-2} and is associated with a wind speed reduction by 28%. We there interpret the results of these two distinct studies as being comparable.

(p) GCM (this study) – Land – Climate model based

The values are taken from this study. The land case corresponds to 26% global coverage, uses a mean pre-turbine wind speed of 4.6 m s^{-1}, a wind speed of 2.6 m s^{-1} at maximum generation (reduced by 44%) with an installed capacity of 24.3 MW_i km^{-2}, generating 0.37 W_e m^{-2} of electricity, which corresponds to 3.2 kWh m^{-2} yr^{-1} or 49 TW_e.

Note that to quantify these values, the installed capacity of 24.3 MW_i km^{-2} is used. This particular simulation was selected as it has the maximum generation rate over land (all Land values shown in Supplement Table 1).

(q) [7] – Land – Climate model based

Miller et al. (2011) considered a land coverage corresponding to 26% global coverage, stated a mean pre-turbine wind speed of 4.3 m s^{-1}, a wind speed of 2.5 m s^{-1} at maximum generation (reduced by 42%), with an installed capacity of 15.2 MW_i km^{-2}, generating 0.26 W_e m^{-2} of electricity, which corresponds to 2.3 kWh m^{-2} yr^{-1} or 34 TW_e.

The GCM used in Miller et al. (2011) is the same as the one being used in this study. We used the values of the simulations with the T42 spectral resolution with 10 vertical levels, as these are consistent with the model setup of this study. A difference in this study is the use of a diurnal cycle in the setup used here.

The setup of Miller et al. (2011) introduces an additional drag coefficient to the lowest atmospheric level over all non-glaciated land surfaces (corresponding to 26% of global surface). The control pre-turbine wind speed of this lowest atmospheric level is not noted in Miller et al. (2011). Similarly, the wind speed corresponding to the maximum generation rate (34 TW_e, or 0.26 W_e m^{-2}) in Miller et al. (2011) was also not stated. A reevaluation of these simulations yield a mean 'pre-turbine' wind speed of 4.3 m s^{-1} and a mean wind speed of 2.5 m s^{-1} (reduced by 42%) at maximum generation. The conversion from the additional drag coefficient of 0.01 as stated in

Miller et al (2011) to an installed capacity (in $MW_i\ km^{-2}$) was done following Gans et al. (2012) and yields an installed capacity of 15.2 $MW_i\ km^{-2}$.

(r) [13] – Land – Climate model based

The number listed corresponds to Jacobson & Archer (2012) for a global coverage of 26%, a mean pre-turbine wind speed of 7.5 m s^{-1}, a wind speed of 4.5 m s^{-1} at maximum generation (reduced by 40%) with an installed capacity of 11.3 $MW_i\ km^{-2}$, generating electricity at a mean rate of 0.54 $W_e\ m^{-2}$, which corresponds to 4.7 kWh $m^{-2}\ yr^{-1}$ or 71 TW_e. Note that a slightly higher generation rate of 72 TW_e is also noted in Jacobson & Archer (2012), but with less information being provided (see also explanation for line m earlier).

Jacobson & Archer (2012) in their Table 1 show that for their Simulation I, an installed capacity of 11.3 $MW_i\ km^{-2}$ over 26% of the global surface generated 71.2 TW_e. The slightly higher generation rate of 72 TW_e (Simulation M) was achieved by increasing the horizontal model resolution from 4ºx5º to 1.5ºx1.5º, but this simulation was only calculated for six months "…due to their enormous computing requirements" (p.15681 of Table 1). Spatial information and area-weighted quantities of generation and wind speed are only provided for the 5 year 4ºx5º Simulation I.

From Supplement Figure S3A, the pre-turbine wind speed over land at 100-meters is noted as 7.48 m s^{-1}. From their Table 1 for Simulation I, the maximum generation rate over land of 71.2 TW_e is achieved with an installed capacity of 11.3 $MW_i\ km^{-2}$.

(s) [20] – Land – Climate model based

The values taken from Wang & Prinn (2010) are listed as 11% global coverage, generating 0.33 $W_e\ m^{-2}$, 2.9 kWh $m^{-2}\ yr^{-1}$, or 19 TW_e.

Wang & Prinn (2010) deploy wind turbines into specific land cover types: grass (including cold C3 and warm C4) and shrub (including evergreen and deciduous), which covered an area of 58 million km^2 (11.4% of global surface). The "computed electrical energy outputs" from the VH (Very High alterations to the pre-turbine surface roughness) is also stated as 603 EJ yr^{-1} or 19 TW_e. The generation rate per unit area then yields 0.33 $W_e\ m^{-2}$ or 2.9 kWh $m^{-2}\ yr^{-1}$.

(t) [4] – Land – Climate model based

The values taken from Keith et al. (2004) are listed as 2.6% global coverage, generating 1.19 $W_e\ m^{-2}$, 10.4 kWh $m^{-2}\ yr^{-1}$, or 16 TW_e.

Keith et al. (2004) added drag to the surface and then quantified "…the additional power dissipated by surface friction due to the additional drag" (p.16116). To estimate electricity generation from this additional dissipation term, Keith et al. (2004) estimate a conversion efficiency of 47-57%. This conversion is quantified in [21] for the simulations in Keith et al. (2004) where 10% of the global land surface (2.6% global surface) is covered by wind turbines (corresponding to an area of $1.3 \cdot 10^{13}\ m^2$). This yields a maximum generation rate of about 1.2 $W_e\ m^{-2}$ (Fig. 4 of [21]). This mean generation rate can be reproduced by applying the 47% conversion efficiency (from additional dissipation to electricity) to the additional dissipation rate of 34 TW attributed to the wind turbines (Fig. 2 in Keith et al., 2004) and dividing it by the 2.6% global coverage area, yielding 1.19 $W_e\ m^{-2}$.

(u) [22] – Land – Climate model based

The values taken from Fitch (2015) are listed as 0.4% global coverage, a mean pre-turbine wind speed of 3.2 m s^{-1}, a wind speed of 2.3 m s^{-1} with wind turbines (reduced by 29%) with an installed capacity of 10 MW_i km^{-2}, generating electricity at a mean rate of 0.63 W_e m^{-2}, which corresponds to 5.5 kWh m^{-2} yr^{-1} or 1.3 TW_e.

Fitch (2015) in Table 3 shows the maximum generation rate of 0.633 W_e m^{-2} or 1.259 TW_e is achieved from the WFD2 simulation, with an installed capacity of 10 MW_i km^{-2} deployed over a total area of $2 \cdot 10^6$ km^2 (corresponding to 0.392% of global coverage). The pre-turbine wind speeds at hub-height and the wind speeds with wind turbines are not stated in the paper. Given that the mean wind speed reduction within the wind farm areas for WFD2 is stated on p.6168 as 0.92 m s^{-1}, and later noted as a mean reduction of 28.8%, the wind speeds at hub-height can be back-calculated to yield a mean pre-turbine control wind speed of 3.19 m s^{-1} and a mean wind speed with wind turbines of 2.27 m s^{-1}.

(v) GCM (this study) – Ocean – Climate model based

The values are taken from this study. They correspond to 71% global coverage, a mean pre-turbine wind speed of 7.8 m s^{-1}, a wind speed of 3.9 m s^{-1} at maximum generation (reduced by 50%) with an installed capacity of 9.1 MW_i km^{-2}, generating electricity at a mean rate of 0.59 W_e m^{-2}, which corresponds to 5.2 kWh m^{-2} yr^{-1} or 213 TW_e.

These values are taken from the sensitivity simulation with an installed capacity of 9.1 MW_i km^{-2}, as this simulation yields the maximum generation rate over ocean. The ocean values for all sensitivity simulations are given in the supplementary material in Table 2.

(w) [13] – Ocean – Climate model based

The values taken from Jacobson & Archer (2012) are listed as 74% global coverage, a mean pre-turbine wind speed of 8.4 m s^{-1}, a wind speed of 4.1 m s^{-1} at maximum generation (reduced by 51%) with an installed capacity of 11.3 MW_i km^{-2}, generating electricity at a mean rate of 0.38 W_e m^{-2}, which corresponds to 3.3 kWh m^{-2} yr^{-1} or 162 TW_e.

Note that Jacobson & Archer (2012) did not explicitly simulate an 'only ocean' wind power scenario. We used the ocean values of their Simulation B, which stated a generation rate of 162 TW_e in their Supplement Figure 3Bi. The control wind speed over the ocean is given as 8.39 m s^{-1} (Supplement Fig. 3A) with a wind speed of 4.09 m s^{-1} at maximum generation (Supplement Fig. 3Bii) resulting from the generation rate of 162 TW_e. The installed capacity of 11.3 MW_i km^{-2} for Simulation B is listed in Table 1.

(x) [20] – Ocean (nearshore) – Climate model based

The values taken from Wang & Prinn (2010) are listed as 2% global coverage, generating electricity at a mean rate of 0.30 W_e m^{-2}, 2.6 kWh m^{-2} yr^{-1}, or 3 TW_e. Wang & Prinn (2010) deploy wind turbines in the shallow ocean (<200m depth) along the coastal boundaries, noted to occupy an area of 10 million km^2 (corresponding to 2.0% of global surface). The "computed electrical energy outputs" from the OH

(Ocean High alterations to the pre-turbine ocean surface roughness) is stated as 30 EJ yr^{-1} or 3 TW_e. The generation rate per unit area is then 0.3 W_e m^{-2}.

(y,z) [23]

The values taken from Wang & Prinn (2011) represent two different studies that differ in the spatial coverage of turbines. In Wang & Prinn (2011), a case was considered in which wind turbines are deployed to coastal regions with depths less than 200 m. This case corresponds to 2.2% global coverage, yielded an estimate of mean electricity generation of 0.61 W_e m^{-2}, 5.3 kWh m^{-2} yr^{-1}, or 6.8 TW_e. The other value in our Table 1 relates to a similar study by these authors where wind turbines were deployed into coastal offshore regions with depths less than 600 m. The values for this study correspond to 3.6% global coverage, an estimated mean electricity generation rate of 0.64 W_e m^{-2}, 5.6 kWh m^{-2} yr^{-1}, or 11.9 TW_e.

Wang & Prinn (2011) state that for their 200H simulation (similar in region to the Wang & Prinn, 2010 study offshore), the deployment area is $11.2 \cdot 10^{12}$ m^2 (corresponding to 2.2% of global coverage). This setup generates 6.8 TW_e of electricity, which corresponds to 0.61 W_e m^{-2} or 5.3 kWh m^{-2} yr^{-1}. Extending this coastal offshore region to include depths up to 600 meters (identified as 600H in Wang & Prinn, 2011) increases the deployment area to $18.5 \cdot 10^{12}$ m^2 (3.6% of global coverage). This setup generates 11.9 TW_e, which corresponds to 0.64 W_e m^{-2} or 5.6 kWh m^{-2} yr^{-1}.

References

[1] Fraedrich K, Jansen H, Kirk E, Luksch U, Lunkeit F (2005) The planet simulation: towards a user friendly model. Meteorol. Z. 14: 299-304

[2] Lunkeit F, et al. (2007) Planet simulator reference manual version 15.0. Meteorological Institute of the University of Hamburg, Hamburg, Germany. https://epic.awi.de/29589/1/Lun2007e.pdf *accessed July 4, 2016*

[3] Miller LM, et al. (2015) Two methods for estimating limits to large-scale wind power generation. Proc Natl Acad Sci USA 112(36) 11169-11174

[4] Keith DW, et al. (2004) The influence of large-scale wind power on global climate. Proc Natl Acad Sci USA 101(46):16115–16120

[5] Gans F, Miller LM, Kleidon A (2012) The problem of the second wind turbine — a note on common but flawed wind power estimation methods. Earth Syst. Dynam 3:79–86

[6] Corten G (2001) Novel views on the extraction of energy from wind: Heat generation and terrain concentration. Proceedings of the 2001 EWEC conference. http://www.ecn.nl/docs/library/report/2001/rx01054.pdf *accessed July 4, 2016*

[7] Miller LM, Gans F, Kleidon A (2011) Estimating maximum global land surface wind power extractability and associated climatic consequences. Earth Syst. Dynam 2:1–12

[8] Hansen K, Barthelmie R, Jensen L, Sommer A (2012) The impact of turbulence intensity and atmospheric stability on power deficits due to wind turbine wakes at Horns Rev wind farm. Wind Energy. 15: 183-196

[9] MacKay DJ (2013) Could energy-intensive industries be powered by carbon-free electricity? Philos Trans A Math Phys Eng Sci 371(1986):20110560

[10] Meneveau C (2012) The top-down model of wind farm boundary layers and its applications. J Turbul 13:1–12

[11] Gustavson M (1979) Limits to wind power utilization. Science 204(4388): 13-17

[12] Jacobson MZ, Delucchi M (2011) Providing all global energy with wind, water, and solar power, Part I: Technologies, energy resources, quantities and areas of infrastructure, and materials. Energy Policy 39:1154–1169

[13] Jacobson MZ, Archer CL (2012) Saturation wind power potential and its implications for wind energy. Proc Natl Acad Sci USA 109(39):15679–15684

[14] Archer C, Jacobson M (2005) Evaluation of global wind power. J Geophys Res 110(D12):D12110

[15] Lu X, McElroy MB, Kiviluoma J (2009) Global potential for wind-generated electricity. Proc Natl Acad Sci USA 106(27):10933–10938

[16] IPCC (2012) IPCC Special Report on Renewable Energy Sources and Climate Change Mitigation. Cambridge University Press, Cambridge (UK) 1076 pp.

[17] Rogner, H et al. (2000). Energy resources. In: *World Energy Assessment. Energy and the Challenge of Sustainability*. United Nations Development Programme, United Nations Department of Economic and Social Affairs, World Energy Council, New York, USA, 508 pp.

[18] Capps S, Zender C (2010) Estimated global ocean wind power potential from QuikSCAT observations, accounting for turbine characteristics and siting. J. Geophys. Res. 115:D09101

[19] Marvel K, Kravitz B, Caldeira K (2013) Geophysical limits to global wind power. Nature Climate Change. 3, 118-121

[20] Wang C, Prinn R (2010) Potential climatic impacts and reliability of very large-scale wind farms. Atmospheric Chemistry and Physics 10:2053-2061

[21] Adams AS, Keith D (2013) Are global wind power resource estimates overstated? Environ Res Lett 8:015021

[22] Fitch A (2015) Climate impacts of large-scale wind farms as parameterized in a global climate model. Journal of Climate 28:6160-6180

[23] Wang C, Prinn R, (2011) Potential climatic impacts and reliability of large-scale offshore wind farms. Environ. Res. Lett. 6, 025101